Burns & Trauma, 2026, **14**, tkag013
https://doi.org/10.1093/burnst/tkag013
Published: 10 February 2026
Research Article

OXFORD

Breaking the vicious cycle of impaired angiogenesis and chronic inflammation in diabetic wounds: a bioengineered microneedle system delivering RGD-modified M2 exosomes

HongYu Wang[1,2], BaoHua Wei[1], BaiShi Wang[1], Mi Chai[1], Jing Ren[1], Yan Han[3], LingLi Guo[1,*]

[1]Department of Plastic and Reconstructive Surgery, First Medical Center of Chinese People's Liberation Army General Hospital, Fuxing Road, Haidian District, Beijing 100853, China
[2]Department of Burn and Plastic Surgery, People's Liberation Army No. 983 Hospital, Huangwei Road, Hebei District, Tianjin 300000, China
[3]Plastic Surgery Department, Peking University International Hospital, District Life Science Park Road, Changping District, Beijing 100853, China
*Corresponding author. E-mail: guo_linglidoctor@163.com

Abstract

Background: **Persistent local tissue hypoperfusion and chronic inflammation are central challenges in diabetic wound management. The development of effective therapeutic strategies to mitigate prolonged inflammation and enhance tissue vascularization is crucial for accelerating diabetic wound healing. This study aimed to develop soluble microneedle materials that simultaneously target both aspects to improve the clinical prognosis of diabetic wounds.**

Methods: **A stable macrophage cell line overexpressing basic fibroblast growth factor (bFGF) was established using lentiviral transfection. After M2 polarization was induced with interleukin-4 (IL-4) and IL-10, exosomes were isolated via ultracentrifugation and surface-functionalized with arginine-glycine-aspartic acid (RGD)-targeting peptides. The reparative effects of these exosomes on human umbilical vein endothelial cells (HUVECs) with high glucose-induced injury were evaluated using scratch test, 5-ethynyl-2′-deoxyuridine (EdU) staining, and cell counting kit-8 assays. A delivery system based on soluble hyaluronic acid microneedles (MNs) loaded with engineered exosomes was then developed. Its therapeutic efficacy was evaluated in a diabetic wound mouse model, and the underlying mechanisms were explored via ribonucleic acid (RNA) sequencing.**

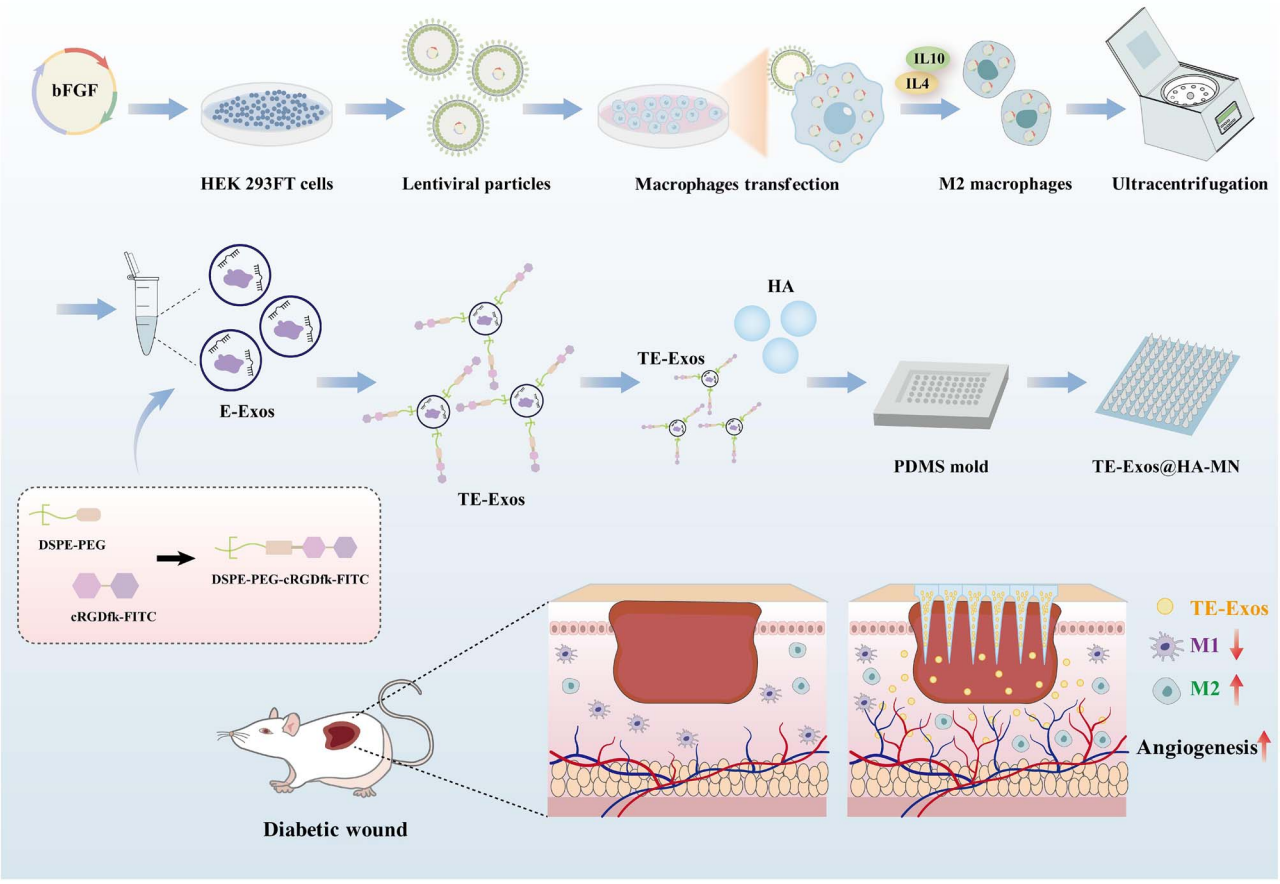
Results: **Targeted engineered exosomes (TE-Exos) derived from bFGF-overexpressing M2 macrophages with surface RGD modification were successfully prepared. Assays revealed that TE-Exos exhibited specific targeting to HUVECs with high glucose-induced injury and significantly enhanced cellular proliferation, migration, and tube formation. Furthermore, the polarization ratio of macrophages improved after TE-Exos treatment. *In vivo*, the MN-mediated delivery of TE-Exos markedly accelerated diabetic wound healing by enhancing re-epithelialization, collagen deposition, and angiogenesis. Furthermore, the treatment modulated the wound microenvironment by reducing the infiltration of proinflammatory M1 macrophages while increasing the proportion of reparative M2 macrophages. RNA sequencing analysis indicated that the therapeutic effects were mediated primarily through the inhibition of excessive inflammation and the activation of angiogenesis-related signaling pathways.**

Conclusions: **This innovative strategy breaks the vicious cycle of impaired angiogenesis and chronic inflammation in diabetic wounds through a synergistic mechanism involving 'angiogenesis, inflammation regulation, and precise delivery'. The combination of targeted exosome engineering with an MN delivery system not only overcomes the limitations of conventional growth factor therapies but also enables intelligent modulation of the wound microenvironment, offering novel theoretical insights and practical approaches for clinical translation.**

Received: 3 September 2025. **Revised:** 18 January 2026. **Accepted:** 5 February 2026
© The Author(s) 2026. Published by Oxford University Press.
This is an Open Access article distributed under the terms of the Creative Commons Attribution-NonCommercial License (https://creativecommons.org/licenses/by-nc/4.0/), which permits non-commercial re-use, distribution, and reproduction in any medium, provided the original work is properly cited. For commercial re-use, please contact reprints@oup.com for reprints and translation rights for reprints. All other permissions can be obtained through our RightsLink service via the Permissions link on the article page on our site—for further information please contact journals.permissions@oup.com.

Downloaded from academic.oup.com/burnstrauma/article/doi/10.1093/burnst/tkag013/8471195 by guest on 12 October 2026

Graphical Abstract



Keywords Diabetic wounds, Targeted engineered exosomes, Microneedles, Macrophage polarization, Wound healing

Highlights

- **The findings of this study indicate that macrophage-derived exosomes engineered through targeted modification exhibit substantial therapeutic potential in the treatment of diabetic wounds.**
- **MNs loaded with targeted engineered exosomes (TE-Exos) effectively promote epithelial tissue proliferation, stimulate collagen synthesis, enhance local angiogenesis, regulate the M1/M2 macrophage balance, and significantly accelerate wound healing in diabetic mice. This innovative strategy breaks the vicious cycle of impaired angiogenesis and chronic inflammation in diabetic wounds through a synergistic mechanism involving 'angiogenesis, inflammation regulation, and precise delivery'.**
- **The integration of targeted exosome engineering with an MN delivery system not only overcomes the limitations of conventional growth factor therapy but also enables intelligent modulation of the wound microenvironment, offering novel theoretical insights and practical approaches for clinical applications.**

Background

Diabetic wounds are among the most common and challenging complications in tissue repair and regeneration [1]. According to the International Diabetes Federation, the global population affected by diabetes is projected to reach 643 million (11.3%) by 2030 and 783 million (12.2%) by 2045. Among these individuals, at least 5%–10% will experience diabetic wound complications [2]. Current clinical treatments remain unsatisfactory, placing a substantial economic burden on both patients and health care systems [3, 4]. The prominent characteristics of diabetic wounds are persistent inflammatory responses and insufficient tissue perfusion, which lead to local skin defects and prolonged healing time [5]. Apart from blood sugar control, perfusion improvement, lifestyle alterations, and other symptomatic treatments, local management plays a pivotal role in the seamless healing of diabetic wounds.

A major limitation of existing therapies is their inability to simultaneously address the two core pathological features of diabetic wounds: a dysregulated inflammatory microenvironment and compromised angiogenesis. To overcome this dual challenge, a multitarget synergistic therapeutic strategy is imperative. A promising candidate for promoting angiogenesis is basic fibroblast growth factor (bFGF); however, its clinical application

Downloaded from academic.oup.com/burnstrauma/article/doi/10.1093/burnst/tkag013/8471195 by guest on 12 October 2026

is severely hampered by its intrinsic instability, short half-life, and rapid degradation in the wound environment, often resulting in subtherapeutic concentrations at the target site [6–12]. These limitations underscore the critical need for a stable and efficient delivery system. Exosomes have emerged as ideal next-generation nanocarriers because of their high biocompatibility, low immunogenicity, and enhanced tissue permeability [13–20]. Specifically, exosomes derived from M2-polarized macrophages (M2-Exos) are advantageous because they serve dual functions: as delivery vehicles and as inherent therapeutic agents. M2-Exo, cargo can reprogram the prevalent proinflammatory M1 macrophages toward the healing M2 phenotype, thereby directly mitigating chronic inflammation-a key pathological feature of diabetic wounds [14, 21–26].

Despite this potential, the therapeutic efficacy of native exosomes is limited by limited targeting specificity and rapid systemic clearance. To address this limitation, we engineered the exosome surface with the arginine-glycine-aspartic acid (RGD) peptide, which specifically binds to integrin $\alpha v\beta 3$-a receptor highly expressed on activated endothelial cells during wound repair and angiogenesis [27–32]. Studies such as those by Liu *et al.* and Gao *et al.* have demonstrated that RGD modification significantly enhances the targeting and therapeutic efficacy of exosomes in promoting vascularization and treating inflammatory conditions [33, 34].

1,2-Distearoyl-SN-propyl-3-phosphatidylethanolamine (DSPE), an amphiphilic phospholipid, is frequently conjugated with polyethylene glycol (PEG) to form DSPE-PEG. This compound is used to improve the stability and targeting ability of exosomes [35]. In this study, DSPE-PEG-cRDGfk-FITC was used as a modified peptide, with the DSPE end binding to the lipid bilayer membrane of engineered exosomes and the RGD sequence at the other end enhancing the targeting of engineered exosomes to blood vessels. Without destroying the structural integrity and biological properties of exosomes, targeted engineered exosomes can be constructed.

Finally, to ensure efficient local delivery, we integrated the targeted exosomes into a soluble hyaluronic acid (HA) microneedle (MN) patch. This platform combines the excellent biocompatibility and drug-carrying capacity of HA with the minimal invasiveness, high delivery efficiency, and strong adhesion of MNs, thereby maximizing local drug enrichment and patient compliance [36–39]. Conventional topical formulations, such as hydrogels and ointments, are largely confined to the wound surface, resulting in low bioavailability at the deeper dermal layers where regeneration and immune regulation primarily occur. This limitation is particularly detrimental for sophisticated therapeutics such as exosomes and growth factors, which require direct access to their cellular targets to exert their full pro-healing effects. Furthermore, the use of a biopolymer such as HA as the MN matrix combines this superior delivery capability with the inherent moist wound-healing benefits of a hydrogel. Upon dissolution, the HA matrix contributes to a favorable wound microenvironment, promoting hydration and cell migration.

We therefore propose an innovative strategy that breaks the vicious cycle of impaired angiogenesis and chronic inflammation through synergistic 'angiogenesis–inflammation modulation–precisely delivery'. The aim of this study was to develop a targeted exosome–MN system and validate its potential to intelligently modulate the wound microenvironment, thereby offering novel insights and a transformative therapeutic platform for diabetic wound care.

Table 1 Primers used for qPCR

Primer	Sequence (5′ to 3′)
Mouse-GAPDH	Forward:AGGTCGGTGTGAACGGATTTG
	Reverse:TGTAGACCATGTAGTTGAGGTCA
Mouse-bFGF	Forward:AGCCTTTTATGTAATAGTAAG (endogenous)
	Forward:GACGATGACAAGTGAGCGAT (exogenous)
	Reverse:GAACTGGGCAGTATAAAC

bFGF basic fibroblast growth factor

Methods

Culture and transfection of RAW264.7 cells

RAW264.7 cells were maintained in Dulbecco's Modified Eagle's Medium (DMEM) supplemented with 10% fetal bovine serum and 1% penicillin/streptomycin at 37.5°C under 5% CO_2. A lentiviral plasmid carrying the bFGF gene was packaged, and the viral supernatant was harvested to infect RAW264.7 cells. Transfected cells were selected using puromycin.

Immunofluorescence staining

Cells were fixed, permeabilized, and blocked. The cells were subsequently incubated with a diluted primary antibody, followed by treatment with the corresponding secondary antibody, and incubated for 1 h at room temperature in the dark. Nuclei were counterstained with 4′,6-diamidino-2-phenylindole (DAPI) for 10 min.

Western blot

Total protein was extracted from lysed cells or tissues and quantified using a bicinchoninic acid assay. Proteins were separated by sodium dodecyl sulfate–polyacrylamide gel electrophoresis (100 V) and transferred to PVDF membranes. After blocking, the membranes were incubated with primary and secondary antibodies. Protein bands were visualized using Super ECL Plus chemiluminescent substrate and imaged with an automated detection system.

Real-time fluorescence quantitative polymerase chain reaction

Gene-specific primers (Table 1) were synthesized by Service Biotechnology. Ribonucleic acid (RNA) was reverse transcribed, and amplification was performed using the QuantStudio™ 3 Real-Time polymerase chain reaction (PCR) System under the following conditions: 94°C for 30 s, followed by 45 cycles of 94°C for 5 s and 60°C for 30 s.

Enzyme-linked immunosorbent assay

Cell culture supernatant and lysates were collected. Cells were washed, resuspended in phosphate-buffered saline (PBS), and sonicated on ice. The samples were subsequently centrifuged at

Downloaded from academic.oup.com/burnstrauma/article/doi/10.1093/burnst/tkag013/8471195 by guest on 12 October 2026

12 000 rpm for 15 min, after which the supernatant was analysed using a commercial enzyme-linked immunosorbent assay (ELISA) kit. The absorbance was measured at 450 nm.

Flow cytometry

Cells were washed twice with cold PBS and resuspended at 1×10^6 cells/ml. The cells were stained with fluorophore-conjugated antibodies for 30 min at room temperature, washed, and resuspended in 500 μl of PBS for analysis.

M2 polarization of macrophages

RAW264.7 cells were seeded in 6-well plates. After 24 h, the medium was replaced with fresh DMEM containing 20 ng/ml interleukin (IL)-4 and 20 ng/ml IL-10. The cells were incubated for 36 h to induce M2 polarization.

Exosome isolation by ultracentrifugation

Cell culture medium was sequentially centrifuged at 500 × g for 10 min and 10 000 × g for 30 min to remove debris. The supernatant was ultracentrifuged at 100 000 × g for 70 min. The pellet was resuspended in Dulbecco's PBS (DPBS) and ultracentrifuged again at 100 000 × g for 120 min. Purified exosomes were resuspended in 200 μl of sterile DPBS.

Transmission electron microscopy

Exosomes were fixed in 2.5% glutaraldehyde for 2 h, adsorbed onto copper grids, and negatively stained with 1.5% uranyl acetate. The grids were air-dried and imaged under transmission electron microscopy (TEM).

Nanoparticle tracking analysis

Samples were diluted in PBS to the appropriate concentrations and injected into the NanoSight chamber. After calibration with polystyrene standards, particle size and concentration were analysed using Nanoparticle tracking analysis (NTA) software.

Establishment of human umbilical vein endothelial cells with high glucose-induced injury

HUVECs were treated with 20 mM glucose and 100 μg/ml advanced glycation end products (AGEs) for 48 h to simulate a diabetic vascular endothelial cell pathology model.

Transwell assay

Matrigel was diluted 1:3 in serum-free medium, and 50 μl was added to the Transwell inserts. The lower chamber contained 600 μl of medium supplemented with 20% fetal bovine serum (FBS). HUVECs (5×10^5 cells/ml) were seeded in the upper chamber and incubated for 24 h. Cells were fixed with 4% platelet function assay and stained with 1% crystal violet.

Synthesis and identification of the arginine-glycine-aspartic acid cyclic peptide

DSPE-PEG2K-NHS (10 mg) was dissolved in 1 ml of dimethylformamide and mixed with cRGDfk-FITC peptide (1.1 equiv) and triethylamine (3.0 equiv). The reaction was carried out at room temperature for 18 h. The product was dialyzed (molecular weight cut-off 2000 Da) and lyophilized. The RGD cyclic peptide was dissolved in dimethyl sulfoxide-d_6 (DMSO-d_6), and a high-resolution ^{1}H-NMR spectrometer was used to perform 50 scans at 25°C.

Synthesis of targeted engineered exosomes

DSPE-PEG-cRGDfk-FITC was dissolved in DMSO and mixed with exosomes (50 μl per 100 μg of exosomes) for 3 h at room temperature. Targeted engineered exosomes (TE-Exos) were purified by ultrafast centrifugation and resuspended in PBS.

Internalization of targeted engineered exosomes by human umbilical vein endothelial cells with high glucose-induced injury

When HUVECs confluence reached 30% and 70% confluence, TE-Exos were added, followed by incubation at room temperature for 3 h. Tubulin staining and DAPI re-staining were performed. FITC fluorescence was observed under a fluorescence microscope to confirm whether the targeted engineered exosomes had successfully entered the HUVECs.

HUVECs with high glucose-induced injury were incubated with PKH26-labeled TE-Exos for 3 h. Cell nuclei were counterstained with DAPI. Following sealing, exosome endocytosis was observed under a fluorescence microscope.

Effects of targeted engineered exosomes on human umbilical vein endothelial cells with high glucose-induced injury

Matrigel (50 μl) was dispensed into 96-well plates and polymerized at 37°C for 30 min. HUVECs and exosomes were resuspended and adjusted to a concentration of $3–5 \times 10^4$ cells/ml. Subsequently, 100 μl of the cell suspension was seeded onto the Matrigel surface and incubated for 4 h. Tubular structures were imaged and analysed.

A total of $0.5–1 \times 10^6$ HUVECs with high glucose-induced injury were seeded into 6-well plates. The 5-ethynyl-2′-deoxyuridine (EdU) assay was performed using an EdU detection kit in accordance with the manufacturer's instructions.

HUVECs with high glucose-induced injury were seeded into 96-well plates. After 24, 48, and 72 h of incubation, 10 μl of cell counting kit-8 (CCK-8) solution was added to each well, followed by incubation at 37°C for 2 h in the dark. The absorbance at 450 nm was measured using a microplate reader.

HUVECs with high glucose-induced injury were seeded into 6-well plates at a density of 5×10^5 cells per well and cultured until

Downloaded from academic.oup.com/burnstrauma/article/doi/10.1093/burnst/tkag013/8471195 by guest on 12 October 2026

~90% confluence. A straight scratch was created in the monolayer using a sterile 100 μl pipette tip. Subsequently, 100 μl of exosomes was added, and the culture was continued. The control group received an equal volume of PBS solution. Cell migration was observed under a microscope at 24 h and 48 h post-scratch. The cell-free gap area was quantified using ImageJ software, and the relative area of scratch closure was calculated as follows: relative area of scratch closure (%) = [(initial wound area - wound area at the time of observation)/initial wound area] $\times$ 100%.

Isolation of mouse peritoneal macrophages

BALB/c mice (6 weeks old) were used in the experiments. Peritoneal inflammation was induced by the intraperitoneal injection of 0.5 ml of 3% thioglycolate broth, followed by aspiration of the peritoneal fluid. In the intervention group, 200 μl of corresponding exosomes (E-Exos or TE-Exos) was administered via intraperitoneal injection. Three days post-treatment, the mice were euthanized by cervical dislocation. Subsequently, 2 ml of precooled RPMI-1640 culture medium was injected into the peritoneal cavity for lavage, and the resulting peritoneal lavage fluid was collected. The fluid was centrifuged, and the cell pellet was resuspended and washed with RPMI-1640 medium. Finally, the polarization status of peritoneal-derived macrophages was assessed using flow cytometry.

Isolation of bone marrow-derived macrophages

Bone marrow was flushed from the femurs and tibias of BALB/c mice. Erythrocytes were lysed, and the cells were cultured for 7 days in M-CSF (20 ng/ml) to differentiate into bone marrow-derived macrophages (BMDMs).

M1 polarization of bone marrow-derived macrophage cells

Macrophage colony-stimulating factor (M-CSF; final concentration, 20 ng/ml) was added to BMDMs cell culture medium for continuous induction over 7 days to induce M0 macrophages. In the control group, no intervention was applied. In the M1 group, the medium was changed to MDM complete medium containing LPS (final concentration of 100 ng/ml) and IFN-γ (final concentration of 50 ng/ml) supplemented with 10% FBS and 1% P/S antibiotics. In the M1/E-Exos group, E-Exos were added in addition to the treatment received by the M1 group intervention. Similarly, in the M1/TE-Exos group, TE-Exos were added in addition to the treatment received by the M1 group. After 48 h of induction culture, the M1 markers CD80 and CD86 and the M2 markers CD206 and CD163 were analysed by flow cytometry.

Preparation and characterization of hyaluronic acid microneedles

Sodium hyaluronate powder was dissolved in purified water or exosome solution. The solution was injected into a polydimethylsiloxane (PDMS) MN mold and spread evenly by moving the mold back and forth. The sodium hyaluronate solution was subsequently introduced into the needle cavities of the PDMS mold using a vacuum negative pressure deaeration technique. The mold was then dried in an oven for 6 h until the MNs could be easily released, yielding HA MNs. The morphology of the MNs was characterized using a scanning electron microscope.

The back skin of BALB/c mice (8 weeks old) was depilated. MNs were then inserted into the skin tissue on the backs of the mice and left in place for 5 min before removal. The skin tissue indented by the MNs was subsequently excised, processed for paraffin embedding, stained with hematoxylin and eosin (HE), and examined under a microscope.

The mechanical strength of the prepared MNs was evaluated using a texture analyser. The MN patch was placed horizontally on the platform with the tips facing upwards. The probe compressed the MN patch vertically at a speed of 0.1 mm/s, and the corresponding compression force was recorded. A standard curve representing the relationship between pressure and displacement was subsequently plotted.

The *in vitro* drug release profile was simulated using bFGF. A solution containing 50 μg/ml bFGF and 50 mg/ml low molecular weight HA was prepared. This solution was subsequently used to fabricate MNs with physically embedded bFGF. The MNs were immersed in 30 ml of sterile deionized water and incubated in a thermostatic shaker (150 rpm, 37°C) to facilitate dissolution. At predetermined time intervals (1, 5, 15, 30, 60, 100, 120, 150, 180, and 200 min), aliquots were collected during the release process. The concentration of released bFGF was quantified using an ELISA kit, and the results were calculated on the basis of both a standard curve and the measured absorbance values.

HUVECs were seeded into a 96-well plate and allowed to attach. The medium was then replaced with bFGF solution, blank MN soaking solution, MN soaking solution loaded with E-Exos, or MN soaking solution loaded with TE-Exos. After incubation for 24 h, cell viability was assessed using CCK-8 assays to evaluate *in vitro* cytotoxicity.

In vivo wound healing in diabetic mice

Diabetic mice (BALB/c) were generated by high-fat diet feeding and STZ injection. A full-thickness circular wound with a diameter of 1.0 cm was created on the dorsal skin of each mouse. The diabetic mice were randomly assigned to four experimental groups (n = 6 per group): the control group, the blank MN group (HA-MN), the E-Exos loaded MN group (E-Exos@HA-MN), and the TE-Exos loaded MN group (TE-Exos@HA-MN). After wound modeling, the mice were subjected to the corresponding treatments. All dressings were secured with 3 M tape. The dressing was changed every other day for 12 days, and the wound healing process was observed and recorded by a camera. The wound healing rate was calculated using the following formula: relative wound area = (wound area on Day 0—wound area on Day t)/wound area on Day 0. The Animal Ethics Committee of the Institute of Radiological Medicine, Chinese Academy of Medical Sciences, approved all animal experiments, ensuring that they were conducted in accordance with its guidelines (Approval number: IRM/2-IACUC-2404-014).

Histological, immunohistochemical, and immunofluorescence analyses

Wound tissues were harvested on Day 12, sectioned, and stained with hematoxylin and eosin (H&E), Masson's trichrome, and

Downloaded from academic.oup.com/burnstrauma/article/doi/10.1093/burnst/tkag013/8471195 by guest on 12 October 2026

anti-CD31 antibodies. Immunofluorescence staining for iNOS and CD206 was performed using tissue sections.

Ribonucleic acid sequencing

RNA sequencing was performed using mouse tissue samples through a series of procedures, including RNA extraction, an assessment of RNA sample quality, library construction, high-throughput sequencing, and subsequent bioinformatics analysis.

Statistical analysis

We used GraphPad Prism 10.0 for data analysis. To compare two groups, we applied Student's t test. When multiple groups were compared, one-way analysis of variance was used. Post hoc pairwise comparisons were conducted using Tukey's honestly significant difference test following a significant one-way analysis of variance (ANOVA) result. If the data did not follow a normal distribution or had uneven variance, we used the Kruskal–Wallis H test. For data involving both time and treatment factors, a two-way ANOVA was employed to assess the main effects and interaction. The data are shown as means ± standard deviation (SD). We considered results to be statistically significant if $P < 0.05$.

Results

M2 polarization of basic fibroblast growth factor-overexpressing macrophages and phenotypic characterization

RAW264.7 cells were successfully transfected with a lentivirus carrying the bFGF gene and a GFP tag. Fluorescence microscopy confirmed robust green fluorescence in the transfected cells, indicating high transfection efficiency (Figure 1a). Immunofluorescence staining revealed intense orange–red signals for intracellular bFGF in the transfected group, confirming successful overexpression at the protein level (Figure 1b). ELISA results further demonstrated that compared with those in the control and empty vector groups, both the cellular and secreted bFGF levels were significantly elevated in the transfected group (Figure 1c and d). Western blot analysis consistently revealed markedly increased bFGF protein expression in the overexpression group (Figure 1e and f). Additionally, qPCR confirmed that expression of the exogenous bFGF mRNA transcript was significantly greater than that of the endogenous gene (Figure 1g). Collectively, these results verify the successful establishment of a stable macrophage line overexpressing bFGF.

Macrophages were polarized to the M2 phenotype (Figure 1h–l). Macrophages overexpressing bFGF exhibited typical morphological changes following M2 polarization (Figure 1h). Western blot analysis revealed a significant increase in the expression of the M2 marker Arg-1 following the induction of polarization in both untransfected and transfected macrophages (Figure 1i and l). Flow cytometry confirmed the upregulation of the expression of the M2 surface markers CD206 and CD163 (Figure 1j and k), indicating successful M2 polarization. Importantly, ELISAs and qPCR confirmed that M2 polarization did not reduce the high level of bFGF expression (Figure 1m-o).

Preparation and characterization of targeted engineered exosomes

TEM revealed that the E-Exos and TE-Exos were round or cup shaped,with size ranging from 50 nm to 150 nm, which is consistent with the typical characteristics of exosomes (Figure 2a). According to the NTA assay results, the average particle size of TE-Exos after RGD cyclic peptide modification was greater than that of E-Exos (Figure 2b). Western blot analysis confirmed the presence of exosomal marke rproteins (CD9 and CD81) and the overexpression of bFGF in both exosome types (Figure 2c–e).

We demonstrated the synthesis and internalization of TE-Exos (Figure 2f–j). Synthesized peptide products were analysed using ^{1}H-NMR mass spectrometry (Figure 2f and h). The results revealed the presence of characteristic signals at corresponding positions: FITC (6.5–8.5 ppm), cRGDfk (4.0–4.8 ppm), PEG (3.6–3.8 ppm), and the fatty acid chain of DSPE (1.3 ppm). These findings confirmed the successful synthesis of the DSPE-PEG-cRGDfk-FITC peptide. This peptide was subsequently conjugated to the surface of E-Exos (from bFGF-overexpressing M2 macrophages) via the hydrophobic DSPE moiety to construct TE-Exos (Figure 2f).

Fluorescence microscopy confirmed the efficient internalization of FITC-labeled TE-Exos by HUVECs with high glucose-induced injury at both 30% and 70% confluence (Figure 2g). A comparative uptake assay using PKH26-labeled exosomes revealed that both E-Exos and TE-Exos were internalized by HUVECs after 6 h of coincubation. However, compared with the E-Exos group, the TE-Exos group demonstrated significantly greater cellular uptake efficiency (Figure 2i and j).

Influence of targeted engineered exosomes on human umbilical vein endothelial cells with high glucose-induced injury

We established an in vitro model of high glucose-induced endothelial injury using HUVECs (Figure S1a–g). Western blot and qPCR analyses confirmed the successful establishment of HUVECs with high glucose-induced injury, as evidenced by the significantly upregulated expression of ICAM-1, NF-κB, and Bax and downregulated expression of Bcl-2 (Figure S1a, b and d). Flow cytometry with Annexin V/PI staining confirmed a significantly higher apoptosis rate in HUVECs with high glucose-induced injury than in control cells (Figure S1e and g). Furthermore, a transwell assay demonstrated that HUVECs with high glucose-induced injury had a severely impaired migratory capacity (Figure S1c and f).

Targeted engineered exosomes significantly ameliorated high glucose-induced dysfunction in HUVECs (Figure 3a–m). As shown in Figure 3, both E-Exos and TE-Exos promoted the tube formation of HUVECs with high glucose-induced injury (the numbers of nodes, junctions, and meshes in both groups were greater than those in the H-AGEs group (Figure 3a-d). At the same time, the tube formation of vascular endothelial cells in TE-Exos group was better than that in E-Exos group (the number of nodes and junctions in the TE-Exos group was not significantly different from that in the E-Exos group, but the number of

Downloaded from academic.oup.com/burnstrauma/article/doi/10.1093/burnst/tkag013/8471195 by guest on 12 October 2026

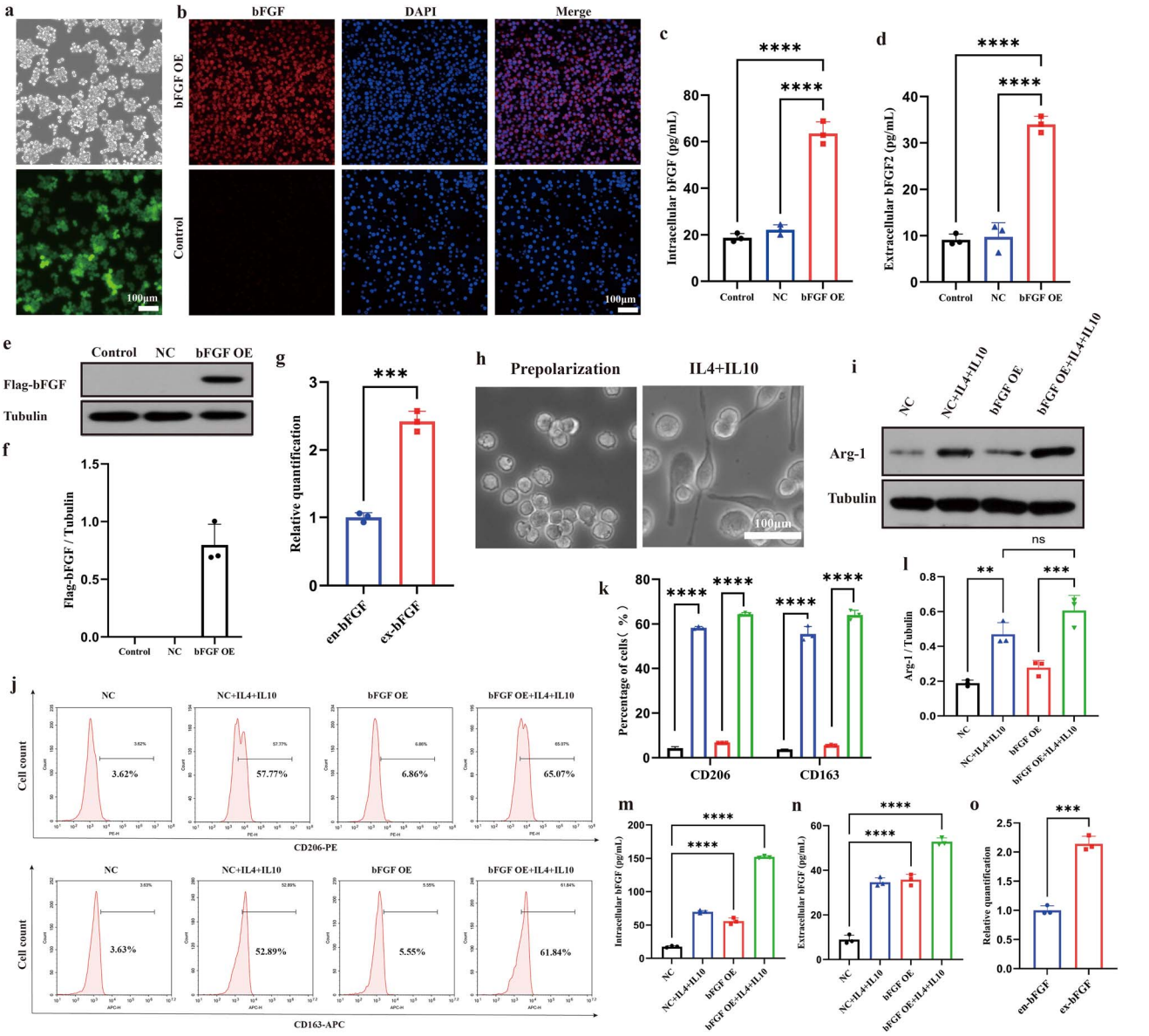


Figure 1 Establishment of stable bFGF overexpressed macrophage cell lines and M2 polarization. (**a**) Green fluorescence was observed in macrophages after transfection (Sale bar: 100 μm). (**b**) Immunofluorescence labeling of bFGF in RAW264.7 cells yielded orange–red fluorescence in the bFGF OE group. (**c**) Intracellular bFGF expression in cell lysate was assessed by ELISAs. (**d**) The concentration of bFGF secreted in the culture medium was measured by ELISAs. (**e** and **f**) Flag-bFGF expression was assessed by western blotting. (**g**) qPCR analysis was performed to determine the ratio of endogenous to exogenous bFGF in bFGF-overexpressing cell lines. (**h**) Morphological changes in transfected RAW264.7 cells before and after M2 polarization (Sale bar: 100 μm). (**i**) Arg-1 expression in polarized cells. (**j** and **k**) Flow cytometry results for the M2 macrophage markers CD206 (PE channel) and CD163 (APC channel). (**l**) Statistical results of Arg-1 expression inpolarized cells. (**m** and **n**) ELISAs were used to quantify intracellular and extracellular bFGF levels after M2 polarization. (**o**) qPCR analysis of endogenous and exogenous bFGF expression following M2 polarization. En-bFGF and ex-bFGF represent the relative expression levels of endogenous bFGF and exogenous flag-bFGF, respectively. NC: no-load plasmid transfection group; bFGF OE: bFGF overexpression group; NC + IL4 + IL10: IL-4 and IL-10 were administered to NC group; bFGF OE + IL4 + IL10: IL-4 and IL-10 were administered to the bFGF overexpression group. $^{**}P < 0.01$, $^{***}P < 0.001$, and $^{****}P < 0.0001$; *ns* no statistically significant difference. *ELISA* enzyme-linked immunosorbent assay, *IL* interleukin, *bFGF* basic fibroblast growth factor, *NC* negative control

meshes in the TE-Exos group was greater than that in the E-Exos group).

The ability of exosomes to promote the proliferation of HUVECs was examined by EdU assays. The results showed that both E-Exos and TE-Exos promoted the proliferation of HUVECs with high glucose-induced injury. Among them, TE-Exos has the most obvious effect on promoting the proliferation of vascular endothelial cells (Figure 3e and i).

According to the results of scratch test of HUVECs with high glucose-induced injury, the effects of promoting cell migration in the TE-Exos group and E-Exos group were better than those in the control group at 24 and 48 h after scratch. Among these groups, the

Downloaded from academic.oup.com/burnstrauma/article/doi/10.1093/burnst/tkag013/8471195 by guest on 12 October 2026

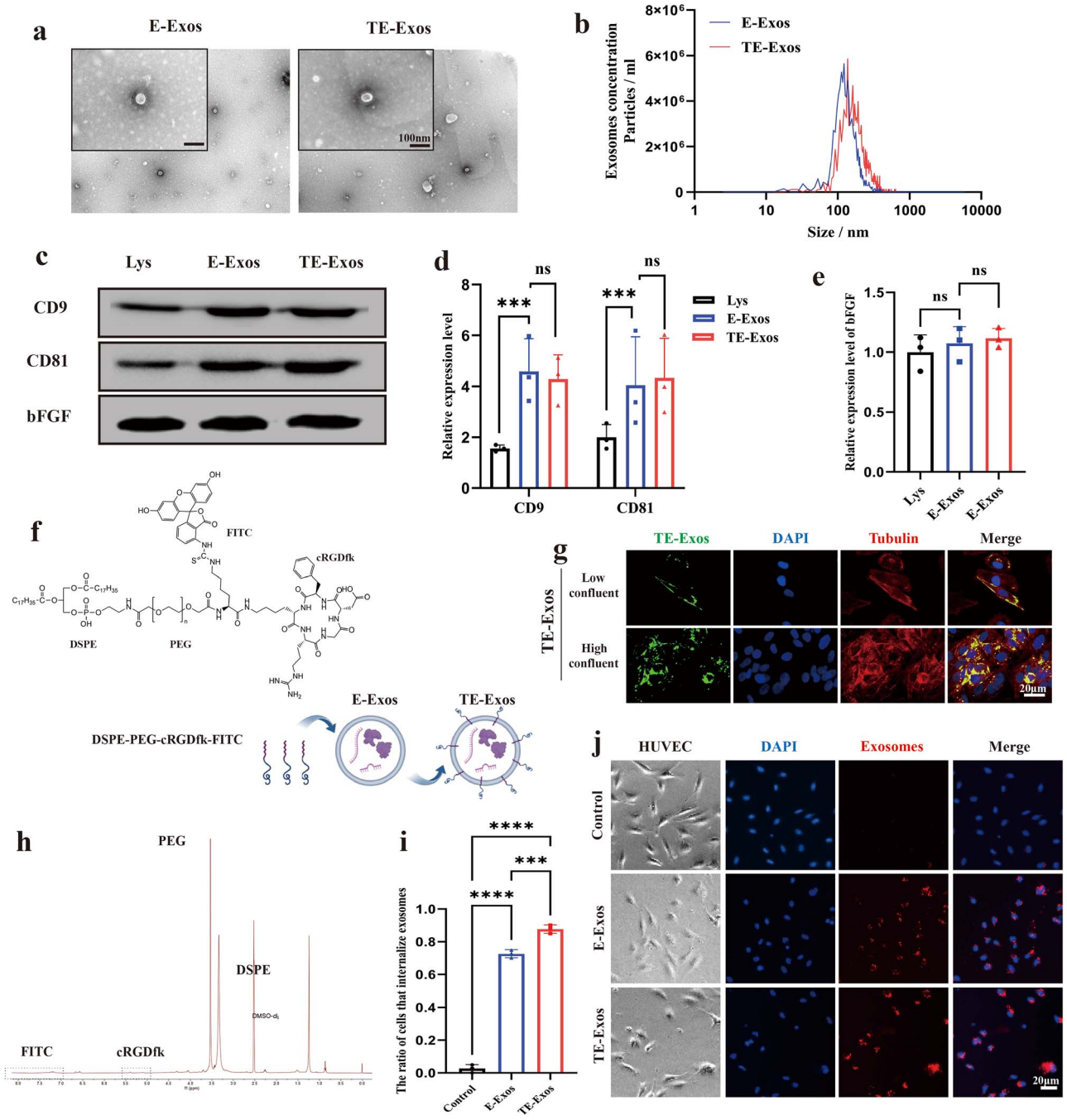


Figure 2 Construction and characterization of TE-exos. (**a**) Exosome morphology was analysed using TEM (Sale bar: 100 μm). (**b**) The NTA results for TE-Exos (red) and E-Exos (blue). (**c-e**) Western blot analysis of the expression levels of the characteristic exosomal proteins CD9, CD81, and bFGF. (**f**) Chemical structural formula of the synthetic DSPE-PEG-cRGDfk-FITC cyclic peptide and schematic diagram illustrating the construction of TE-Exos. (**g**) Internalization of TE-Exos by HUVECs. Low confluent indicates a cell confluence of 30%, whereas high confluent indicates a cell confluence of 70%. Green fluorescence corresponds to FITC in the RGD cyclic peptide, and tubulin is stained red (Sale bar: 20 μm). (**h**) 1H-NMR mass spectrometry results for DSPE-PEG-cRGDfk-FITC, with DMSO-d6 as the deuterated solvent for dissolving the cyclic peptide. (**i** and **j**) Internalization of PKH26-labeled exosomes by HUVECs with high glucose-induced injury (Sale bar: 20 μm). Exosomes are stained red, and nuclei are stained blue (DAPI); *Lys* macrophage lysate. $^{***}P < 0.001$ and $^{****}P < 0.0001$; *ns* no statistically significant difference. *ELISA* enzyme-linked immunosorbent assay, *IL* interleukin, *bFGF* basic fibroblast growth factor

ability of TE-Exos to promote vascular endothelial cell migration was stronger than that of E-Exos (Figure 3f-h).

CCK-8 assays revealed that the OD value of the ordinate was positively correlated with the number of living cells. The results in Figure 3j-m showed that both E-Exos and TE-Exos significantly induced the proliferation of HUVECs with high glucose-induced injury. At the 24-h node, the effect in the TE-Exos group was not significantly different from that in the E-Exos group, but after 48 and 72 h, the effect in the TE-Exos group was significantly greater than that in the E-Exos group.

Downloaded from academic.oup.com/burnstrauma/article/doi/10.1093/burnst/tkag013/8471195 by guest on 12 October 2026

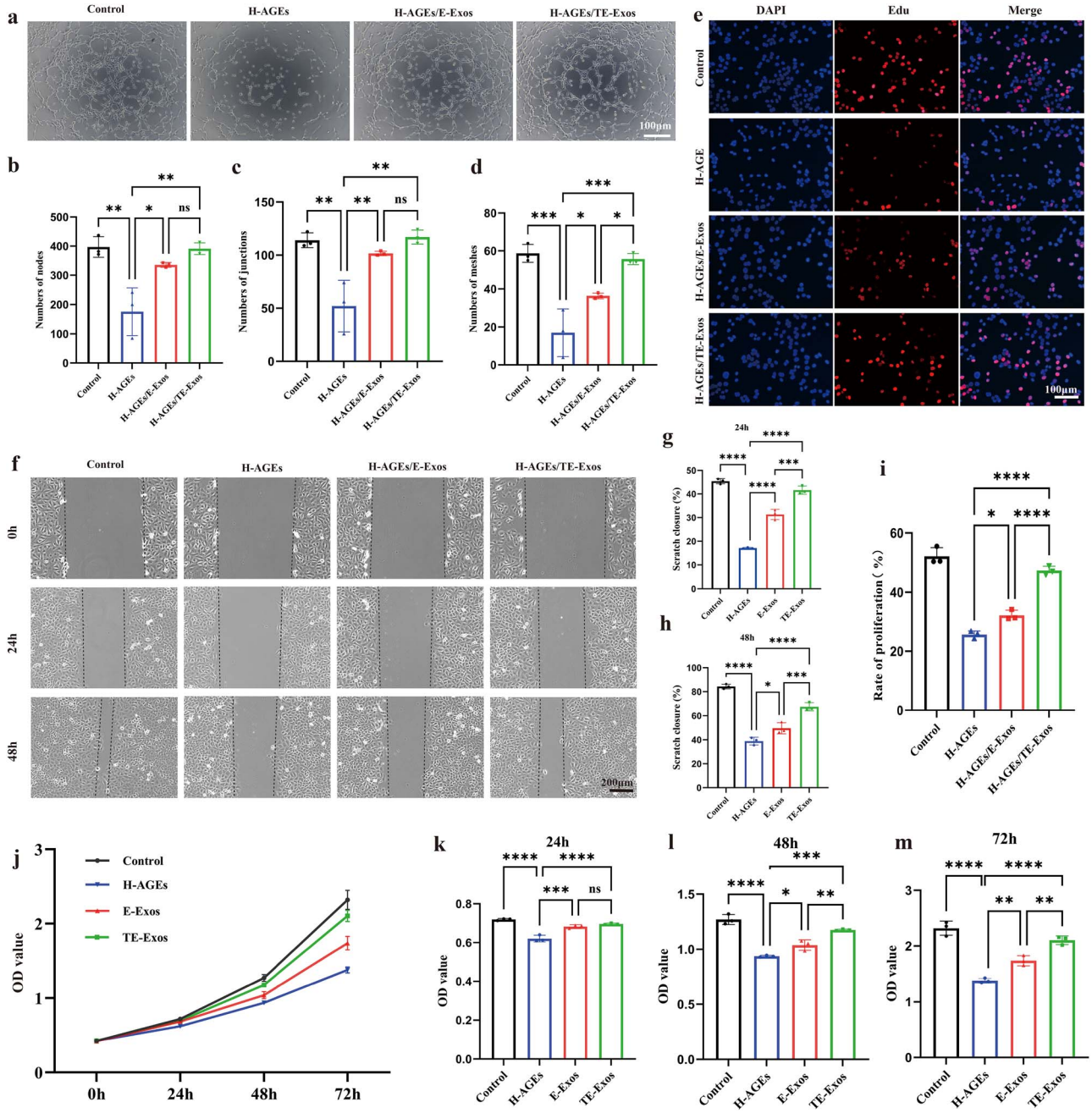


Figure 3 Effects of exosomes on HUVECs with high glucose-induced injury. (**a-d**) The ability of exosomes to promote HUVEC tube formation (Sale bar: 100 μm). (**e**) EdU assay results for assessing the ability of exosomes to promote HUVEC proliferation. The DAPI column shows nuclei (Sale bar: 100 μm). (**f-h**) Scratch assay results for HUVECs. (**i**) The statistical results of the Edu assay (Sale bar: 100 μm). (**j**) CCK-8 assays assessing the effect of exosomes on the proliferation of HUVECs. (**k-m**) Comparison of OD values at 24, 48, and 72 h. Control: HUVECs; H-AGEs: HUVECs with high glucose-induced injury; H-AGEs/E-Exos: HUVECs with high glucose-induced injury treated with E-Exos; H-AGEs/TE-Exos: HUVECs with high glucose-induced injury treated with TE-Exos. $^{*}P < 0.05$, $^{**}P < 0.01$, $^{***}P < 0.001$, and $^{****}P < 0.0001$; *ns* no statistically significant difference. *TE-Exos* targeted engineered exosomes, *E-Exos* engineered exosomes, *TEM* transmission electron microscopy, *HUVECs* human umbilical vein endothelial cells

Effect of targeted engineered exosomes on the polarization ratio of macrophages

The results revealed that the M1/M2 polarization ratio of peritoneal macrophages differed among the groups that received different interventions. In the control group, the expression levels of M1-type macrophage markers (CD86 and CD80) were the highest, while those of M2-type macrophage markers (CD206 and CD163) were the lowest, resulting in the highest M1/M2 ratio. Following treatment with TE-Exos, the expression levels of CD86 and CD80 in mouse peritoneal macrophages decreased, whereas the expression levels of CD206 and CD163 increased (Figure 4a-c). Consequently, treatment with TE-Exos led to a reduction in the M1/M2 ratio of mouse peritoneal macrophages.

Treatment with LPS and IFN-γ led to significant increases in the expression levels of CD80 and CD86 in BMDMs,

Downloaded from academic.oup.com/burnstrauma/article/doi/10.1093/burnst/tkag013/8471195 by guest on 12 October 2026

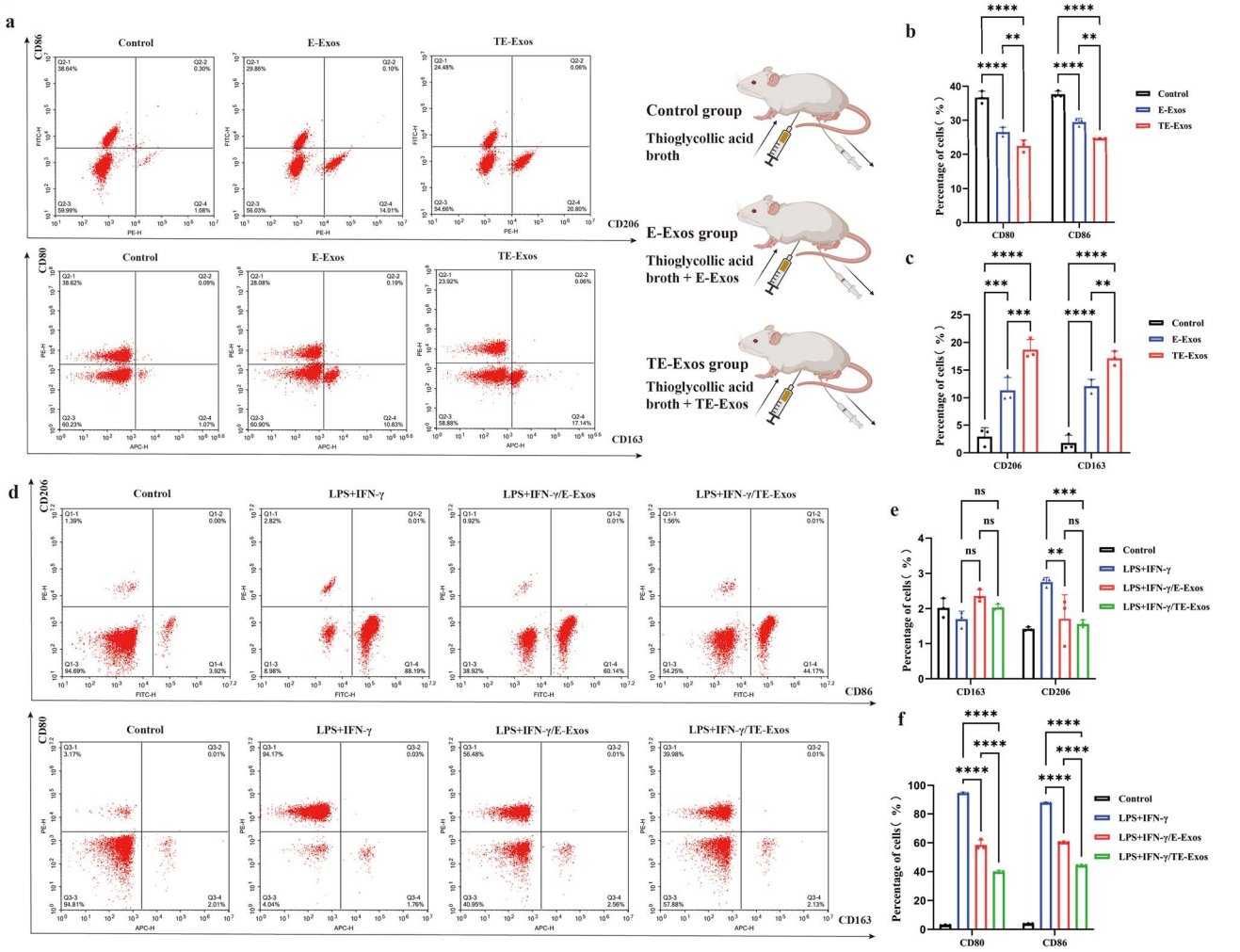


Figure 4 Effect of TE-Exos on the polarization of macrophages. (**a-c**) Effect of TE-Exos on the polarization ratio of peritoneal macrophages in mice. (b and c) Expression levels of M1 or M2 macrophage markers. (**d**) Influence of TE-Exos on M1 polarization of BMDMs. (**e** and **f**) Expression levels of M1 or M2 macrophage markers. The PE channel indicates the expression levels of CD206 and CD80, while the FITC and APC channels represent the expression of CD86 and CD163, respectively; $^{**}P < 0.01$, $^{***}P < 0.001$, and $^{****}P < 0.0001$; *ns* no statistically significant difference. *AGEs* advanced glycation end products, *E-Exos* engineered exosomes, *DAPI* 4′,6-diamidino-2-phenylindole, *OD* optical density

confirming their successful polarization toward the M1 phenotype. When TE-Exos were administered in combination with LPS and IFN-γ, the expression levels of CD80 and CD86 significantly decreased, whereas the expression of CD163 and CD206 slightly decreased (Figure 4d-f). Consequently, the overall M1/M2 macrophage ratio decreased after treatment with TE-Exos.

Preparation and characterization of soluble hyaluronic acid microneedles

HA MNs were prepared by PDMS MN mold and the vacuum negative pressure deportation method. The prepared MN patches were square and transparent, with a side length of 2 cm and 20 × 20 MNs in each patch. Each MN has a length of ∼250 μm, a circular base, and a diameter of 150 μm (Figure 5a). Each MN patch contains ∼3–5 × 10^{10} exosomes.

The indentation results of the MNs applied to the dorsal skin of the mice are presented in Figure 5b. Upon penetrating the skin, the MNs severed the epidermis and some subcutaneous tissue. The MNs penetrated the tissue to a depth of ∼200–250 μm, corresponding to their total length.

The displacement of a single MN under various mechanical forces is shown in Figure 5c. When the compression displacement reached 600 μm, the stress exerted on the MNs prepared in this study exceeded 0.30 N. The mechanical force required for a single MN to penetrate the skin was 0.045 N, whereas the force required to penetrate the wounded granulation tissue was even lower. These results indicate that the HA MNs developed in our study possess excellent mechanical properties and can penetrate wound tissue effectively.

The HA-MN system showed no cytotoxicity (Figure 5d) and exhibited rapid release kinetics, with most of the loaded cargo released within 200 minutes (Figure 5e).

TE-exos@HA-MN promote diabetic wound healing

On the 12th day post-wounding in diabetic mice, varying degrees of epithelial tissue growth were observed, with the defect being

Downloaded from academic.oup.com/burnstrauma/article/doi/10.1093/burnst/tkag013/8471195 by guest on 12 October 2026

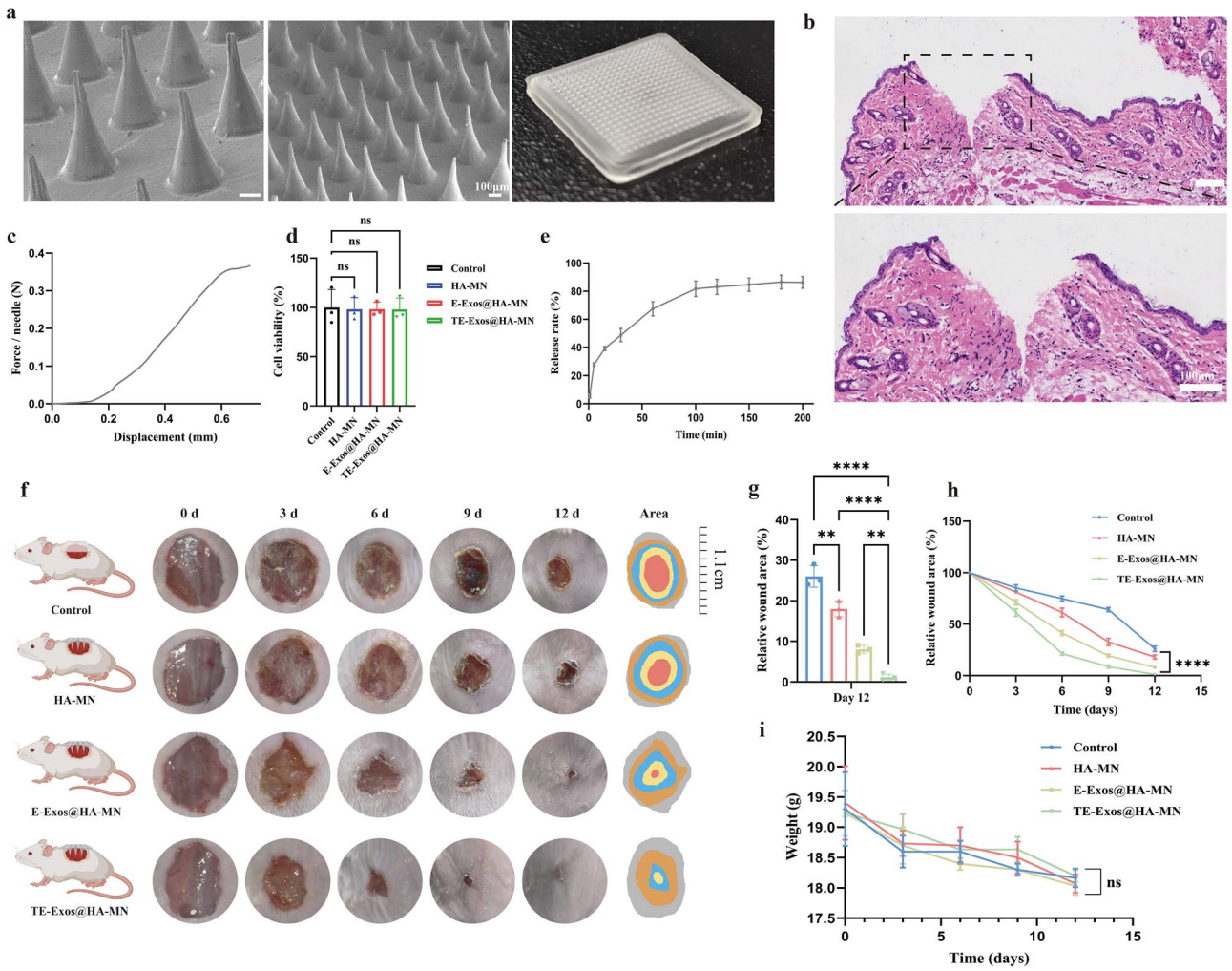


Figure 5 Characterization and application of TE-Exos@HA-MN in diabetic mice. (**a**) The morphology of hyaluronic acid MNs observed under scanning electron microscopy (Scale bar: 100 μm). (**b**) Indentation of hyaluronic acid MNs into mouse skin. The depth of the insertion of the MN tip into the skin ranged from ~200–250 μm (Scale bar: 100 μm). (**c**) Mechanical properties of the hyaluronic acid MNs. The horizontal axis represents the displacement distance of the MNs, whereas the vertical axis indicates the mechanical force exerted on each MN; *N* newtons; (**d**) Cell compatibility of hyaluronic acid MNs. No significant difference in cell viability was observed between the E-Exos@HA-MN and TE-Exos@HA-MN groups compared with the control group. (**e**) Dissolution and release characteristics of hyaluronic acid MNs. The loaded exosomes were gradually released, with most of the content being released within 200 min. (**f**) Effect of TE-Exos@HA-MNs on wound healing speed in diabetic mice. (**g**) Statistical analysis of changes in the wound area on Day 12. (**h**) Statistical analysis of changes in the wound area ($n = 6$). (**i**) Changes in the body weight of mice across all groups ($n = 6$). **** $P < 0.0001$; *ns* no statistically significant difference. *TE-Exos* targeted engineered exosomes, *HA* hyaluronic acid, *MN* microneedle

either completely or partially filled. Compared with that in the control group, epithelial tissue growth in the E-Exos@HA-MN group and TE-Exos@HA-MN group was significantly better, with noticeable differences observed between Days 3 and 6 post-treatment. Specifically, the TE-Exos@HA-MN group exhibited the fastest healing speed, followed by the E-Exos@HA-MN group, which performed better than the HA-MN group alone (Figure 5f–h). No significant differences in body weight were observed among the treatment groups (Figure 5i). These results demonstrated that TE-Exos@HA-MN significantly enhanced wound healing in diabetic mice.

The results demonstrated that the skin thickness of the control group was the weakest after healing, whereas the skin of the HA-MN, E-Exos@HA-MN, and TE-Exos@HA-MN groups was significantly thicker than that of the control group. Among these groups, the TE-Exos@HA-MN group had the greatest epithelial thickness, which was superior to that of the E-Exos@HA-MN group, indicating that the ability of the TE-Exos@HA-MN to promote epithelialization was greatest. Additionally, the E-Exos@HA-MN group exhibited more granulation tissue formation (Figure 6a and b).

At 12 days post-wounding, compared with the other groups, the TE-Exos@HA-MN group exhibited the deepest collagen staining, with collagen fibers arranged more regularly and densely. In contrast, the control group displayed histological features of collagen deficiency, with a more disorganized arrangement, which hindered tissue repair. Furthermore, both the E-Exos@HA-MN group and the TE-Exos@HA-MN group showed increased capillary-like structures (Figure 6a and c).

By immunohistochemical staining, we observed denser and thicker newly formed capillaries in both the E-Exos@HA-MN group and the TE-Exos@HA-MN group. Notably, the TE-Exos@HA-MN group outperformed all other groups and the HA-MN group also

Downloaded from academic.oup.com/burnstrauma/article/doi/10.1093/burnst/tkag013/8471195 by guest on 12 October 2026

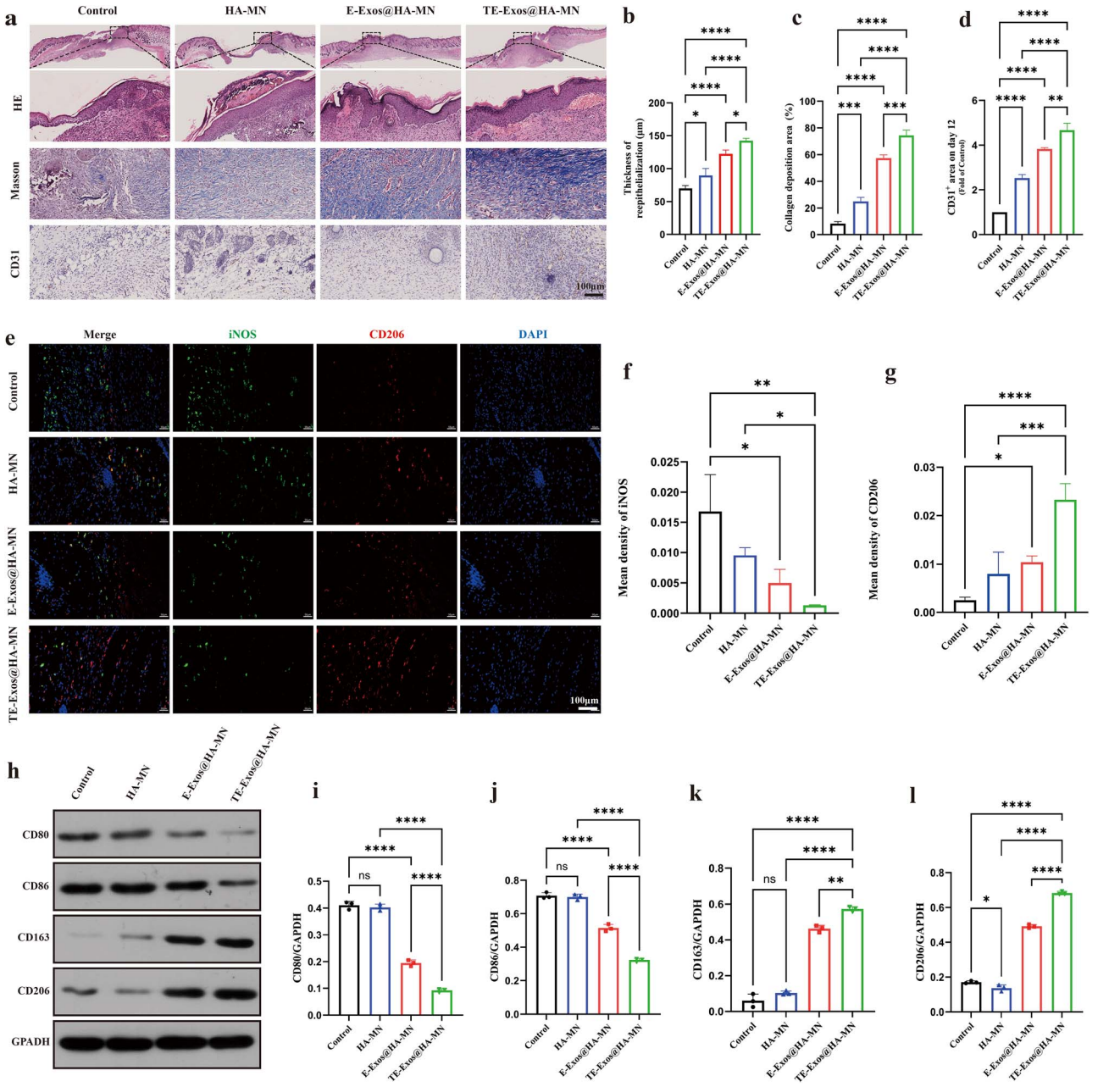


Figure 6 Analysis of wound tissue and detection of macrophage markers. (**a**) H&E and Masson staining were performed using wound skin tissues collected from different groups on Day 12 (black scale bar: 100 μm). Immunohistochemical staining was used to detect platelet endothelial cell adhesion molecule-1 (CD31). (**b**) Reepithelialization thickness on Day 12 ($n = 3$). (**c**) Collagen deposition in the wound on Day 12 ($n = 3$). (**d**) CD31 staining intensity in the wound on Day 12 ($n = 3$). (**e-g**) Immunofluorescence analysis of macrophage markers in tissues, green: iNOS, red: CD206 (Sale bar: 100 μm). (**h**) Western blot analysis was conducted to assess the expression levels of macrophage markers in wound tissue. (**i-l**) Statistica analysis of the expression levels of CD80, CD86, CD163, and CD206, respectively ($n = 3$). $^{*}P < 0.05$, $^{**}P < 0.01$, $^{***}P < 0.001$, $^{****}P < 0.0001$; *ns* no statistically significant difference. *H&E* hematoxylin and eosin, *TE-Exos* targeted engineered exosomes, *HA* hyaluronic acid, *MN* microneedle

exhibited better angiogenesis compared to the control group. These findings suggest that the application of TE-Exos@HA-MN significantly promoted neovascularization in the wound (Figure 6a and d).

Immunofluorescence staining was employed to assess the expression of macrophage polarization markers in tissue samples. The results demonstrated that the expression level of the M1 macrophage marker iNOS was highest in the control group and lowest in the TE-Exos group. Conversely, the expression pattern of the M2 marker CD206 was opposite to that of iNOS (Figure 6e-g).

Consistent with the immunofluorescence results, western blot analysis of wound tissues from Day 12 revealed that the TE-Exos@HA-MN group had the lowest expression levels of M1 markers (CD80 and CD86) and the highest expression levels of M2 markers (CD163 and CD206), indicating a pronounced shift toward a pro-reparative macrophage phenotype (Figure 6h-l).

RNA sequencing revealed a distinct global gene expression profile in the TE-Exos@HA-MN group compared with the other groups (Figure 7a and b). Transcriptome sequencing revealed differentially expressed genes associated with wound healing (Figure 7c-e), including those involved in inflammatory regulation

Downloaded from academic.oup.com/burnstrauma/article/doi/10.1093/burnst/tkag013/8471195 by guest on 12 October 2026

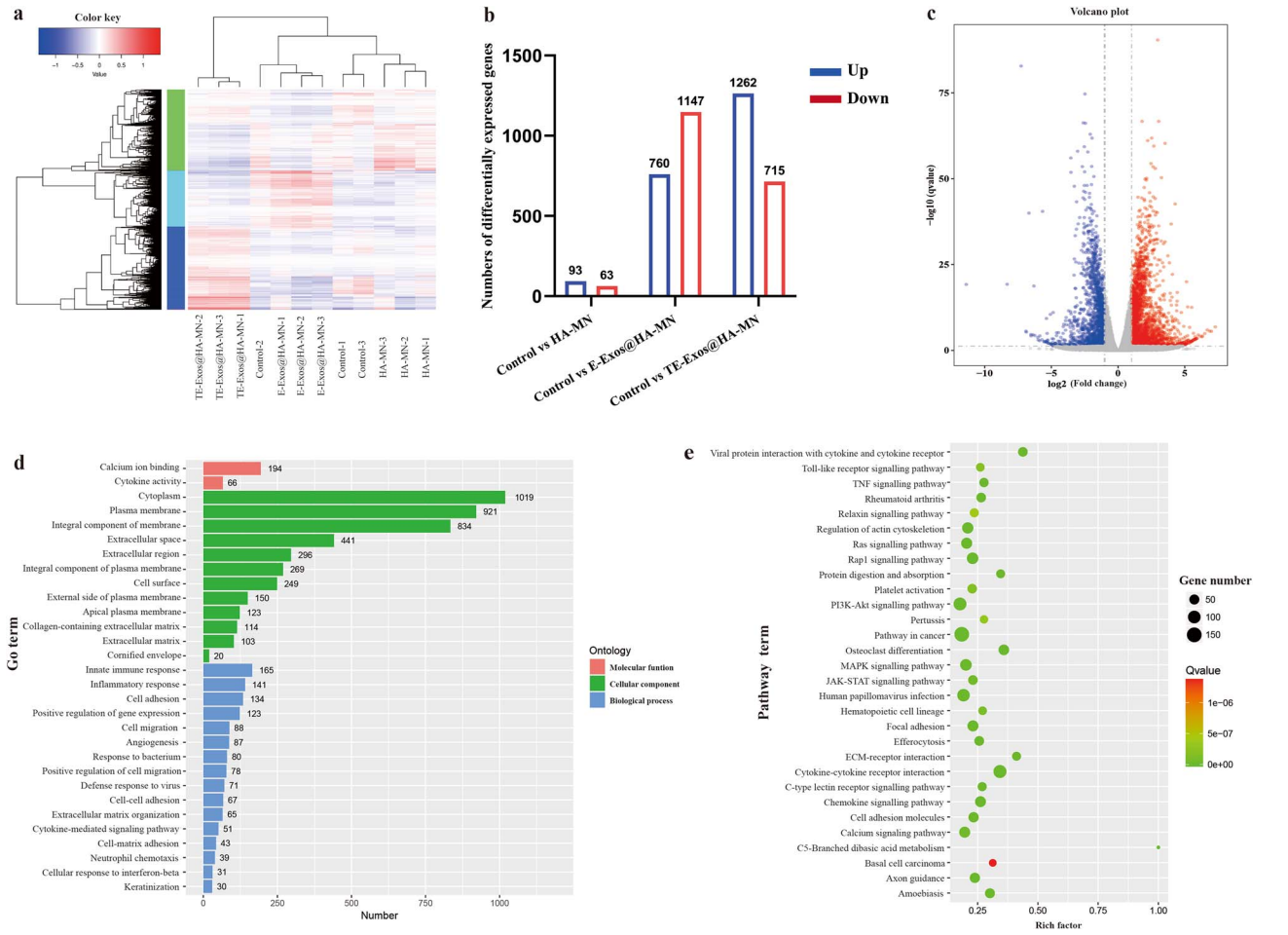


Figure 7 RNA sequencing analysis of wounds. (**a**) Clustered heatmap of tissue gene expression. (**b**) Number of differentially expressed genes between different groups. (**c**) Volcano plot showing the differences in gene expression between the E-Exos@MN group and the TE-Exos@MN group. (**d**) GO analysis of the differentially expressed genes between the E-Exos@MN group and the TE-Exos@MN group. (**e**) KEGG analysis of the differentially expressed genes between the E-Exos@MN group and the TE-Exos@MN group. *RNA* ribonucleic acid, *E-Exos* engineered exosomes, *TE-Exos* targeted engineered exosomes, *MN* microneedle, *GO* gene ontology, *KEGG* kyoto encyclopedia of genes and genomes

and immune response (TNF-α, TLR4, IL-1α, and C5ar1), cell proliferation (TGF-β1, FGF1, HGF, and NGF), extracellular matrix remodeling (MMP13 and CTSL), angiogenesis (NOS2, HMOX1, and ANGPT4), immune cell differentiation (ARG1, STAT4, and CD80), cell adhesion and migration (ICAM-1 and ITGA5), and signaling pathway regulation (Wnt2B and PIK3CG). Western blot and qPCR validation confirmed consistent expression patterns for nine genes (Wnt2B, TNF-α, TLR4, TGF-β1, NOS2, ICAM-1, HGF, CD80, and C5ar1) across both methods Western blot analysis corroborated these findings (Figure 8).

Discussion

Diabetic wounds represent a profound and growing clinical challenge and are pathologically pathological characterized by vascular insufficiency, chronic inflammation, and impaired cellular repair. This study introduces a comprehensive strategy targeting these core mechanisms through the development of TE-Exos delivered via a dissolvable HA MN system. Our findings demonstrate that this combination approach not only enhances angiogenic processes but also effectively reprograms the pathological immune microenvironment of the wound, leading to significantly improved healing outcomes.

The foundation of our approach lies in leveraging the natural biological properties of exosomes. We successfully established a stable bFGF-overexpressing macrophage cell line through lentiviral transduction. This strategy aligns with emerging efforts to genetically modify parent cells to enhance exosome therapeutic potential [40–43]. Crucially, these modified macrophages retained their capacity for M2 polarization, allowing us to obtain exosomes that combine the innate immunomodulatory properties of M2-derived vesicles with enhanced angiogenic signaling via bFGF overexpression. This dual functionality addresses two fundamental pathological features of diabetic wounds simultaneously.

A critical innovation in our study involves the application of active targeting through RGD peptide modification. The RGD tripeptide sequence is a key component of the extracellular matrix (ECM) that specifically binds to various integrins, including integrin $\alpha v\beta 3$ [44]. Angiogenesis, a complex process that requires the coordinated action of multiple factors, heavily relies on integrin activity [45, 46]. Integrin $\alpha v\beta 3$ is an important cell surface receptor in the integrin family; it is composed of two

Downloaded from academic.oup.com/burnstrauma/article/doi/10.1093/burnst/tkag013/8471195 by guest on 12 October 2026

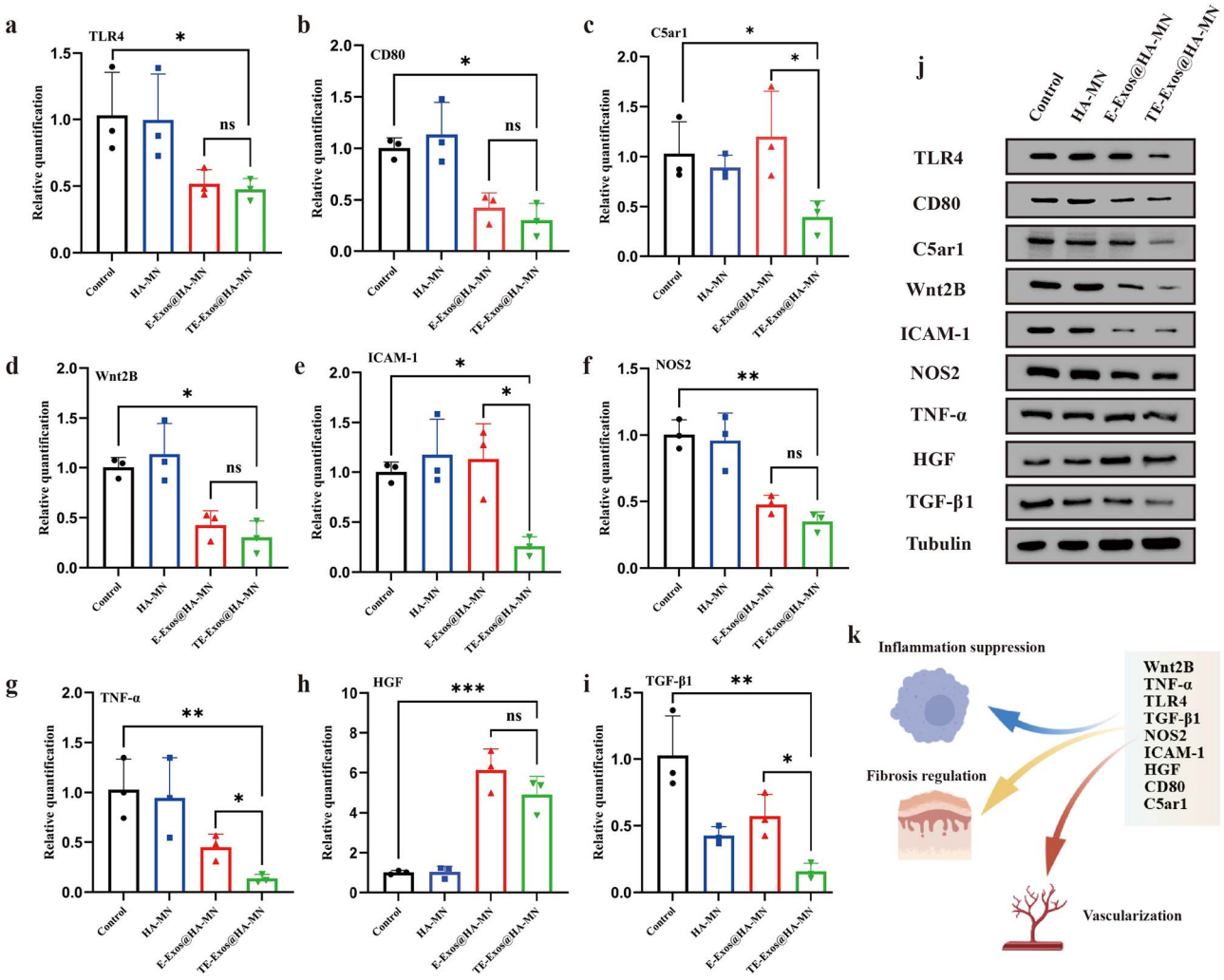


Figure 8 Validation of differentially expressed genes by qPCR and western blot. (**a–i**) Validation of differentially expressed genes by qPCR ($n = 3$). (**j**) Validation of differentially expressed genes by western blotting. (**k**) Schematic diagram of the main functions of the differentially expressed genes. $^{*}P < 0.05$, $^{**}P < 0.01$, $^{***}P < 0.001$; *ns* no statistically significant difference. *TNF-α* tumor necrosis factor-α, *TGF-β1* transforming growth factor-β1, *HGF* hepatocyte growth factor

noncovalently associated type I transmembrane glycoprotein subunits, αv and β3 [47]. Integrin αvβ3 plays a central role in numerous physiological and pathological processes, particularly during angiogenesis and wound healing; it is highly expressed in neovascularization-associated endothelial cells and serves as a receptor for endothelial cell binding to fibronectin in the ECM, thereby promoting vascular formation and stability through the mediation of endothelial cell–ECM interactions [48]. Under resting conditions, endothelial cells exhibit low levels of integrin αvβ3 expression. However, stimulation by factors such as bFGF, vascular endothelial growth factor receptor (VEGFR), and interleukin-8 (IL-8) upregulates its expression. This upregulation also activates matrix metalloproteinase-2 (MMP-2) at the leading edge of neovascularization, facilitating extracellular matrix degradation and enhancing endothelial cell migration and infiltration [49, 50]. Additionally, collagen hydrolysis in the ECM exposes the RGD motif as a ligand for integrin αvβ3, enabling adhesive interactions that provide survival signals and traction for incoming endothelial cells [51, 52].

Therefore, targeting molecules based on RGD can achieve precise drug delivery and enhance therapeutic efficacy [53]. Moreover, compared with linear RGD polypeptides, RGD cyclic peptides (e.g. cRGDfk) exhibit stronger vascular targeting [54]. In this study, we conjugated DSPE-PEG-cRGDfk-FITC peptides to the exosome surface for targeted delivery to vascular endothelial cells. The molecular structure of the RGD cyclic peptide sequence, which primarily includes the DSPE segment, PEG segment, cRGDfk segment, and FITC segment, is illustrated in Figure 5a. Among these, cRGDfk is a five-membered cyclic peptide formed by arginine, glycine, aspartic acid, D-type phenylalanine, and lysine (Arg-Gly-Asp-D-Phe-Lys) via an N-to-C-terminal amide bond to create a ring structure [55]. The DSPE terminus of the targeting peptide can be inserted into and stabilized within the exosome membrane, while FITC serves as a green fluorescent fragment. As a commonly used saturated phospholipid molecule, DSPE plays a critical role in targeted modification because of its excellent biocompatibility and ability to integrate into lipid bilayer membranes [56]. By acting as a

Downloaded from academic.oup.com/burnstrauma/article/doi/10.1093/burnst/tkag013/8471195 by guest on 12 October 2026

linker, DSPE interacts with lipid molecules in the bilayer membrane through its hydrophobic tail to form stable associations [57]. Targeting molecules tethered via DSPE (such as RGD peptides or antibodies) can confer specific targeting capabilities to exosomes. These targeting molecules recognize and bind to specific receptors on target cell surfaces, thereby improving exosome uptake efficiency in target cells and enhancing therapeutic outcomes. Additionally, DSPE insertion enhances exosome membrane stability, preventing rupture or fusion in physiological environments. This helps maintain exosome integrity and biological activity, prolonging their residence time *in vivo* and improving therapeutic efficacy.

In addition to exerting angiogenic effects, TE-Exos demonstrated remarkable immunomodulatory effects. Macrophage polarization is a critical component of immune regulation and plays pivotal roles in immune modulation, tissue remodeling, and the maintenance of metabolic homeostasis [58]. Macrophages are typically classified into two main phenotypes: M1 macrophages, which exhibit proinflammatory properties, and M2 macrophages, which are associated with tissue repair and remodeling [59–61]. Studies have indicated indicates that exosomes derived from M2 macrophages may promote macrophage reprogramming via specific signaling pathways, potentially contributing to inflammation resolution and tissue repair [14]. Exosomes have been developed as drug delivery carriers because of their low immunogenicity, low cytotoxicity, and high stability [62, 63]. Through mechanisms such as membrane fusion, endocytosis, or ligand–receptor interactions [64], exosomes transfer bioactive components including nucleic acids, proteins, and lipids, mediating intercellular communication and regulating metabolic processes [65]. Their specific functions often depend on their cellular source, reflecting the characteristics of their parent cells.

Studies have demonstrated that certain cell-derived exosomes can regulate macrophage polarization, thereby shifting the M1-mediated inflammatory response toward M2-driven tissue repair [14, 66]. For instance, MSC-derived exosomes deliver specific miRNAs (e.g. miR-146a and miR-181c) to inhibit proinflammatory signaling pathways, promoting macrophage M2 polarization [13, 18]. Exosomes derived from M2-type macrophages can accelerate diabetic wound healing by inducing macrophage reprogramming and suppressing inflammatory responses. Macrophage-derived exosomes are preferentially internalized by macrophages, enabling more effective macrophage reprogramming. In essence, exosomes exhibit a preference for their source cells, conferring the advantage of achieving targeted reprogramming in recipient cells [22]. On the basis of this phenomenon, macrophages were selected as the source cells for exosome production in this study to increase the ability of macrophages to undergo M2 phenotype transformation.

However, natural exosomes face limitations in disease therapy and drug delivery because of their variable abundance across tissues and lack of intrinsic targeting specificity [67–70]. These limitations are particularly relevant in diabetic conditions where hyperglycemia impairs HUVEC function, reducing their activity, proliferation, migration ability, and exosome uptake efficiency [71–73]. Under hyperglycemic conditions, the oxidative stress response of vascular endothelial cells increases, which may lead to a decrease in cell membrane fluidity, thus affecting the uptake efficiency of exosomes [74–76]. Hyperglycemia may also affect the functional status of exosome-secreting cells (such as endothelial cells and immune cells), resulting in changes in exosome contents. These changes may affect the role of exosomes in vascular endothelial cells, such as by promoting the inflammatory response and inhibiting cell proliferation. Our results show that targeted modification enhances the uptake of engineered exosomes by injured vascular endothelial cells, facilitating improved function. TE-Exos more effectively promoted the proliferation, migration, and tube formation of vascular endothelial cells under high-glucose conditions, providing a robust foundation for vascular preparation in wound repair.

For clinical translation, we developed an HA MN delivery system that addresses several wound therapy challenges. As fast and direct methods of drug delivery, MNs have attracted increasing attention and been a focus of research in recent years [77]. They deliver drugs to the inside of the skin or a wound, for example, by penetrating the skin barrier or granulation tissue, thereby improving the efficiency and permeability of drug delivery. HA is a naturally occurring polymer acid mucopolysaccharide in human and animal tissues [78]. It is widely present in the extracellular matrix of skin and is the material basis of tissue rheology, hygroscopicity and viscoelastic properties [79]. The application of HA in wound repair has attracted increasing attention because of its ability to provide a moist wound environment, promote cell proliferation and migration, and accelerate re-epithelialization [80]. HA can also stimulate the proliferation and differentiation of fibroblasts and epidermal cells, promote collagen synthesis and deposition, contribute to wound repair and regeneration, and reduce the formation of scar tissue [81, 82]. Moreover, it also has a certain anti-inflammatory effect, which can reduce the inflammatory response of the wound, reduce exudation and edema, and facilitate wound healing [39, 83]. These properties make soluble HA MNs ideal carriers for TE-Exos.

Our experimental results confirmed that the developed HA MNs fully penetrated the skin layer, reaching the subcutaneous tissue and enhancing drug delivery and release. MNs loaded with engineered exosomes demonstrated robust pro-healing effects in diabetic mouse wound models through synergistic effects during the healing process. TE-Exos@HA-MN administration led to a reduced M1-type macrophage proportion and an increased M2-type macrophage proportion, modulating the polarization balance within the wound microenvironment and facilitating the transition from the inflammatory phase to the proliferative healing phase.

A comparative analysis between the TE-Exos@HA-MN and E-Exos@HA-MN groups revealed the significant differential expression of genes enriched in pathways related to inflammation regulation, immune response, cell proliferation, and migration. The expression profiles of these genes suggest that both the E-Exos@HA-MN and the TE-Exos@HA-MN effectively suppressed excessive inflammatory responses, promoted cell proliferation and tissue regeneration, enhanced angiogenesis, and modulated macrophage polarization. Notably, compared with conventional exosomes, TE-Exos@HA-MN exhibited superior therapeutic efficacy. This was evidenced by significantly reduced expression levels of TNF and C5ar1 in the TE-Exos@HA-MN group, indicating a more potent suppression of inflammatory signaling and a more favorable microenvironment for wound repair. Furthermore, decreased ICAM-1 expression suggests reduced inflammatory immune cell infiltration, whereas decreased TGF-β1 expression during the healing phase may help prevent excessive collagen

Downloaded from academic.oup.com/burnstrauma/article/doi/10.1093/burnst/tkag013/8471195 by guest on 12 October 2026

deposition and pathological scar formation. A detailed investigation into the specific signaling pathways (e.g. PI3K/Akt for angiogenesis and STAT3/NF-κB for immunomodulation) activated by TE-Exos constitutes an important direction for our future research.

When our TE-Exos@HA-MN system is contextualized within the current landscape of diabetic wound therapies, its multitargeted and integrative design philosophy becomes a key differentiator. Conventional clinical options, such as silver-based dressings, primarily offer passive antimicrobial protection with limited pro-healing capacity, and advanced biologic growth factors have poor stability and a high cost. Recent pioneering research has opened new avenues by addressing specific healing barriers with high precision [84, 85]. For instance, glycosaminoglycans from *Andrias davidianus* were shown to brilliantly reprogram macrophage glucolipid metabolism, thereby resolving inflammation and promoting repair [86]. In a separate groundbreaking material design, an asymmetric natural nanofiber inspired by the same creature demonstrated rapid temperature-responsive detachment, offering an intelligent solution to the secondary injury often caused by dressing changes [87].

Our strategy is designed to integrate the strengths of such targeted biological modulation and smart material design into a unified platform. Unlike the singular focus of the aforementioned studies, our system involves a synergistic healing cascade. The HA-MN array provides a painless and efficient intradermal delivery vehicle, overcoming the penetration barrier. The engineered TE-Exos then act as multifunctional biological 'nanosurgeons'. Therefore, by converging precision delivery (via MN), active targeting (via RGD), and multimodal therapy (angiogenesis + immunomodulation), our work transcends the limitations of single-mechanism approaches and represents significant progress toward comprehensive and intelligent wound management.

Conclusions

The findings of this study demonstrate that the targeted engineering of macrophage-derived exosomes has significant therapeutic potential for diabetic wound treatment. The MN-mediated delivery of TE-Exos effectively promotes epithelial proliferation, stimulates collagen synthesis, enhances local angiogenesis, and restores the M1/M2 macrophage balance, culminating in markedly accelerated wound healing in diabetic mice. This innovative strategy disrupts the vicious cycle of impaired angiogenesis and chronic inflammation through a synergistic mechanism encompassing 'angiogenesis modulation, immunoregulation, and targeted delivery'. The integration of engineered exosomes with a biocompatible MN system not only surmounts the limitations of conventional growth factor therapies but also enables the precise and intelligent manipulation of the wound microenvironment, offering novel theoretical foundations and practical strategies for clinical translation. Future efforts to develop exosomes derived from macrophages of specific polarization states may further increase therapeutic efficacy for refractory wounds, representing a challenging yet highly promising direction for translational medicine.

Author contributions

HongYu Wang (Conceptualization [lead], Data curation [lead], Investigation [lead], Writing—original draft [equal], Formal analysis [equal], Methodology [equal], Supervision [equal]), Baohua Wei (Formal analysis [equal], Methodology [equal], Investigation [equal], Writing—original draft [equal]), BaiShi Wang (Investigation [equal], Validation [equal], Visualization [equal], Supervision [equal]), Mi Chai (Project administration [equal], Formal analysis [equal], Visualization [equal]), Jing Ren (Project administration [equal], Software [equal], Supervision [equal], Formal analysis [equal]), Yan Han (Resources [lead], Software [equal], Project administration [equal], Writing—review & editing [equal], Supervision [equal]), and LingLi Guo (Writing—original draft [lead], Writing—review & editing [lead], Project administration [equal])

Supplementary material

Supplementary material is available at *Burns & Trauma Journal* online.

Conflict of interest

All the authors declare that they have no conflicts of interest.

Funding

This study was supported by the Tianjin key research and development project (25YFXTHZ00250), special project for cultivating and enhancing the service capacity of traditional Chinese medicine (2023ZY045) and military logistics research (specialized health care project, 23BJZ22).

Data availability

The data are available from the corresponding author on reasonable request.

Ethics approval and consent to participate

The Animal Ethics Committee of the Institute of Radiological Medicine, Chinese Academy of Medical Sciences, approved all animal experiments, ensuring that they were conducted in accordance with its guidelines (Approval number: IRM/2-IACUC-2404-014).

References

1. Holl J, Kowalewski C, Zimek Z, Fiedor P, Kaminski A, Oldak T, *et al.* Chronic diabetic wounds and their treatment with skin substitutes. *Cells* 2021;10:655. https://doi.org/10.3390/cells10030655.
2. B EJ, I.D.A.t.e.s.c, Magliano DJ. *IDF Diabetes Atlas [Internet]*10th edn. Brussels: International Diabetes Federation, 2021.
3. Xiao J, Zhu Y, Huddleston S, Li P, Xiao B, Farha OK, *et al.* Copper metal–organic framework nanoparticles stabilized with folic acid improve wound healing in diabetes. *ACS Nano* 2018;12:1023–32. https://doi.org/10.1021/acsnano.7b01850.

Downloaded from academic.oup.com/burnstrauma/article/doi/10.1093/burnst/tkag013/8471195 by guest on 12 October 2026

4. Armstrong DG, Ingelfinger JR, Boulton AJM, Bus SA. Diabetic foot ulcers and their recurrence. *N Engl J Med* 2017;376:2367–75. https://doi.org/10.1056/NEJMra1615439.
5. Burgess JL, Wyant WA, Abdo Abujamra B, Kirsner RS, Jozic I. Diabetic wound-healing science. *Medicina* 2021;57:1072. https://doi.org/10.3390/medicina57101072.
6. Hou S, Shi Z, Li X, Yang R, Song Y, Zeng Z. Combined negative pressure wound therapy with new wound dressings to repair a ruptured giant omphalocele in a neonate: a case report and literature review. *BMC Pediatr* 2025;25:44. https://doi.org/10.1186/s12887-024-05261-5.
7. Oshima J, Shibuya Y, Sasaki K, Sekido M. Effect of basic fibroblast growth factor in perifascial areolar tissue transplant, Indian. *J Plast Surg* 2024;57:S9–15. https://doi.org/10.1055/s-0044-1787561.
8. Li Y, Ge Z, Liu Z, Li L, Song J, Wang H, *et al.* Integrating electrospun aligned fiber scaffolds with bovine serum albumin-basic fibroblast growth factor nanoparticles to promote tendon regeneration. *J Nanobiotechnol* 2024;22:799. https://doi.org/10.1186/s12951-024-03022-1.
9. Akita S, Hayashida K, Takaki S, Kawakami Y, Oyama T, Ohjimi H. The neck burn scar contracture: a concept of effective treatment. *Burns Trauma* 2017;5:22. https://doi.org/10.1186/s41038-017-0086-8.
10. Jin W, Shen S, Xu X, Xie X, Zhou X, Su X, *et al.* All-in-one hydrogel patches with sprayed bFGF-loaded GelMA microspheres for infected wound healing studies. *Int J Pharm* 2024;658:124205.
11. Zare R, Abdolsamadi H, Soleimani Asl S, Radi S, Bahrami H, Jamshidi S. The bFGF can improve angiogenesis in oral mucosa and accelerate wound healing. *Rep Biochem Mol Biol* 2023;11:547–52. https://doi.org/10.52547/rbmb.11.4.547.
12. Chen G, An N, Ye W, Huang S, Chen Y, Hu Z, *et al.* bFGF alleviates diabetes-associated endothelial impairment by down-regulating inflammation via S-nitrosylation pathway. *Redox Biol* 2021;41:101904.
13. Li X, Liu L, Yang J, Yu Y, Chai J, Wang L, *et al.* Exosome derived from human umbilical cord mesenchymal stem cell mediates MiR-181c attenuating burn-induced excessive inflammation. *EBioMedicine* 2016;8:72–82. https://doi.org/10.1016/j.ebiom.2016.04.030.
14. Kim H, Wang SY, Kwak G, Yang Y, Kwon IC, Kim SH. Exosome-guided phenotypic switch of M1 to M2 macrophages for cutaneous wound healing. *Adv Sci* 2019;6:1900513. https://doi.org/10.1002/advs.201900513.
15. Shi Y, Kang X, Wang Y, Bian X, He G, Zhou M, *et al.* Exosomes derived from bone marrow stromal cells (BMSCs) enhance tendon-bone healing by regulating macrophage polarization. *Med Sci Monit* 2020;26:e923328. https://doi.org/10.12659/MSM.923328.
16. Yang F, Cai D, Kong R, Bi Y, Zhang Y, Lei Y, *et al.* Exosomes derived from cord blood Treg cells promote diabetic wound healing by targeting monocytes. *Biochem Pharmacol* 2024;226:116413.
17. Xu Z, Ni T, Zhang Q, Sun X, Zhao L, Lin J, *et al.* Exosomes derived from fibroblasts in DFUs delay wound healing by delivering miR-93-5p to target macrophage ATG16L1. *Biochim Biophys Acta Mol Basis Dis* 2025;1871:167640. https://doi.org/10.1016/j.bbadis.2024.167640.
18. Yin D, Shen G. Exosomes from adipose-derived stem cells regulate macrophage polarization and accelerate diabetic wound healing via the circ-Rps5/miR-124-3p axis. *Immun Inflamm Dis* 2024;12. https://doi.org/10.1002/iid3.1274.
19. Xu CB, Xu Z, Yu C, Jiang Z. Hydrogel loaded with exosomes from Wharton's jelly-derived mesenchymal stem cells enhances wound healing in mice. *Zhejiang Da Xue Xue Bao Yi Xue Ban* 2023;52:766–76. https://doi.org/10.3724/zdxbyxb-2023-0316.
20. Shi R, Jin Y, Zhao S, Yuan H, Shi J, Zhao H. Hypoxic ADSC-derived exosomes enhance wound healing in diabetic mice via delivery of circ-Snhg11 and induction of M2-like macrophage polarization. *Biomed Pharmacother* 2022;153:113463.
21. Xiong Y, Chen L, Liu P, Yu T, Lin C, Yan C, *et al.* All-in-one: multifunctional hydrogel accelerates oxidative diabetic wound healing through timed-release of exosome and fibroblast growth factor. *Small* 2022;18:2104229. https://doi.org/10.1002/smll.202104229.
22. Kwak G, Cheng J, Kim H, Song S, Lee SJ, Yang Y, *et al.* Sustained exosome-guided macrophage polarization using hydrolytically degradable PEG hydrogels for cutaneous wound healing: identification of key proteins and MiRNAs, and sustained release formulation. *Small* 2022;18(15):e2200060.
23. Deng Y, Xie J, Xiao J, Huang X, Cao Z. Gelatin methacryloyl hydrogel encapsulating molybdenum-inspired macrophage-derived exosomes accelerates wound healing via immune regulation and angiogenesis. *Int J Biol Macromol* 2025;291:138947.
24. X MJJ, Xue K, Chen J, Zhang Y, Zhang G, Wang K, *et al.* Highly bioactive MXene-M2-exosome nanocomposites promote angiogenic diabetic wound repair through reconstructing high glucose-derived immune inhibition. *ACS Nano* 2024;18:4269–86. https://doi.org/10.1021/acsnano.3c09721.
25. Zhang Y, Fang M, Xie W, Zhang Y-A, Jiang C, Li N, *et al.* Sprayable alginate hydrogel dressings with oxygen production and exosome loading for the treatment of diabetic wounds. *Int J Biol Macromol* 2023;242:125081.
26. Cassetta L, Cassol E, Poli G. Macrophage polarization in health and disease. *Sci World J* 2011;11:2391–402. https://doi.org/10.1100/2011/213962.
27. Somanath PR, Malinin NL, Byzova TV. Cooperation between integrin $\alpha v\beta 3$ and VEGFR2 in angiogenesis. *Angiogenesis* 2009;12:177–85. https://doi.org/10.1007/s10456-009-9141-9.
28. Naik MU, Mousa SA, Parkos CA, Naik UP. Signaling through JAM-1 and $\alpha v\beta 3$ is required for the angiogenic action of bFGF: dissociation of the JAM-1 and $\alpha v\beta 3$ complex. *Blood* 2003;102:2108–14.
29. Trimm E, Red-Horse K. Vascular endothelial cell development and diversity. *Nat Rev Cardiol* 2022;20:197–210. https://doi.org/10.1038/s41569-022-00770-1.
30. Marziano C, Genet G, Hirschi KK. Vascular endothelial cell specification in health and disease. *Angiogenesis* 2021;24:213–36. https://doi.org/10.1007/s10456-021-09785-7.
31. Matsushige C, Kitazumi K, Beaman A, Miyagi M, Tallquist MD, Yamazaki Y. RGD peptide promotes follicle growth through integrins $\alpha v\beta 3/\alpha v\beta 5$ in three-dimensional culture. *Reproduction* 2024;169.

Downloaded from academic.oup.com/burnstrauma/article/doi/10.1093/burnst/tkag013/8471195 by guest on 12 October 2026

32. Taledaohan A, Tuohan MM, Jia R, Wang K, Chan L, Jia Y, *et al.* An RGD-conjugated prodrug nanoparticle with blood–brain–barrier penetrability for neuroprotection against cerebral ischemia–reperfusion injury. *Antioxidants* 2024;13:1339. https://doi.org/10.3390/antiox13111339.
33. Wang J, Li W, Lu Z, Zhang L, Hu Y, Li Q, *et al.* The use of RGD-engineered exosomes for enhanced targeting ability and synergistic therapy toward angiogenesis. *Nanoscale* 2017;9:15598–605. https://doi.org/10.1039/c7nr04425a.
34. Tian T, Zhang H-X, He C-P, Fan S, Zhu Y-L, Qi C, *et al.* Surface functionalized exosomes as targeted drug delivery vehicles for cerebral ischemia therapy. *Biomaterials* 2018;150:137–49. https://doi.org/10.1016/j.biomaterials.2017.10.012.
35. Feng W, Teng Y, Zhong Q, Zhang Y, Zhang J, Zhao P, *et al.* Biomimetic grapefruit-derived extracellular vesicles for safe and targeted delivery of sodium thiosulfate against vascular calcification. *ACS Nano* 2023;17:24773–89. https://doi.org/10.1021/acsnano.3c05261.
36. Yang H, Song L, Sun B, Chu D, Yang L, Li M, *et al.* Modulation of macrophages by a paeoniflorin-loaded hyaluronic acid-based hydrogel promotes diabetic wound healing. *Mater Today Bio* 2021;12:100139.
37. Li S, Wang X, Yan Z, Wang T, Chen Z, Song H, *et al.* Microneedle patches with antimicrobial and immunomodulating properties for infected wound healing. *Adv Sci* 2023;10. https://doi.org/10.1002/advs.202300576.
38. Marinelli L, Cacciatore I, Costantini E, Dimmito MP, Serra F, Di Stefano A, *et al.* Wound-healing promotion and anti-inflammatory properties of carvacrol prodrugs/hyaluronic acid formulations. *Pharmaceutics* 2022;14:1468. https://doi.org/10.3390/pharmaceutics14071468.
39. Liang C, Wang R, He T, Chen D, Zhang G, Yin X, *et al.* Revolutionizing diabetic wound healing: the power of microneedles. *CJPRS* 2023;5:185–94.
40. Farhangniya M, Samadikuchaksaraei A. A review of genes involved in wound healing. *Med J Islam Repub Iran* 2023;37:140. https://doi.org/10.47176/mjiri.37.140.
41. Guo L, Xiao D, Xing H, Yang G, Yang X. Engineered exosomes as a prospective therapy for diabetic foot ulcers. *Burns Trauma* 2024;12:tkae023. https://doi.org/10.1093/burnst/tkae023.
42. Morabbi A, Karimian M. Therapeutic potential of exosomal lncRNAs derived from stem cells in wound healing: focusing on mesenchymal stem cells. *Stem Cell Res Ther* 2025;16:62. https://doi.org/10.1186/s13287-025-04200-0.
43. Wu S, Zhou Z, Li Y, Jiang J. Advancements in diabetic foot ulcer research: focus on mesenchymal stem cells and their exosomes. *Heliyon* 2024;10:e37031. https://doi.org/10.1016/j.heliyon.2024.e37031.
44. Bogdanović B, Fagret D, Ghezzi C, Montemagno C. Integrin targeting and beyond: enhancing cancer treatment with dual-targeting RGD (arginine–glycine–aspartate) strategies. *Pharmaceuticals* 2024;17:1556.
45. Stryker ZI, Rajabi M, Davis PJ, Mousa SA. Evaluation of angiogenesis assays. *Biomedicines* 2019;7:37. https://doi.org/10.3390/biomedicines7020037.
46. Golestani R, Jung J-J, Sadeghi M. Molecular imaging of angiogenesis and vascular remodeling in cardiovascular pathology. *J Clin Med* 2016;5:57. https://doi.org/10.3390/jcm5060057.
47. Gu Y, Dong B, He X, Qiu Z, Zhang J, Zhang M, *et al.* The challenges and opportunities of $\alpha v\beta 3$-based therapeutics in cancer: from bench to clinical trials. *Pharmacol Res* 2023;189:106694.
48. Liolios C, Sachpekidis C, Kolocouris A, Dimitrakopoulou-Strauss A, Bouziotis P. PET diagnostic molecules utilizing multimeric cyclic RGD peptide analogs for imaging integrin $\alpha v\beta 3$ receptors. *Molecules* 2021;26:1792. https://doi.org/10.3390/molecules26061792.
49. Rocha LA, Learmonth DA, Sousa RA, Salgado AJ. $\alpha v\beta 3$ and $\alpha 5\beta 1$ integrin-specific ligands: from tumor angiogenesis inhibitors to vascularization promoters in regenerative medicine? *Biotechnol Adv* 2018;36:208–27. https://doi.org/10.1016/j.biotechadv.2017.11.004.
50. Brooks PC, Clark RAF, Cheresh DA. Requirement of vascular integrin $\alpha v\beta 3$ for angiogenesis. *Science* 1994;264:569–71. https://doi.org/10.1126/science.7512751.
51. Robinson SD, Hodivala-Dilke KM. The role of $\beta 3$-integrins in tumor angiogenesis: context is everything. *Curr Opin Cell Biol* 2011;23:630–7. https://doi.org/10.1016/j.ceb.2011.03.014.
52. Davis GE. Affinity of integrins for damaged extracellular matrix: $\alpha v\beta 3$ binds to denatured collagen type I through RGD sites. *Biochem Biophys Res Commun* 1992;182:1025–31.
53. Basirinia G, Ali M, Comelli A, Sperandeo A, Piana S, Alongi P, *et al.* Theranostic approaches for gastric cancer: an overview of *in vitro* and *in vivo* investigations. *Cancers* 2024;16:3323.
54. Yu Y-P, Wang Q, Liu Y-C, Xie Y. Molecular basis for the targeted binding of RGD-containing peptide to integrin $\alpha V\beta 3$. *Biomaterials* 2014;35:1667–75. https://doi.org/10.1016/j.biomaterials.2013.10.072.
55. Deepak P, Kumar P, Pandey P, Arya DK, Jaiswal S, Kumar A, *et al.* Pentapeptide cRGDfK-surface engineered nanostructured lipid carriers as an efficient tool for targeted delivery of tyrosine kinase inhibitor for battling hepatocellular carcinoma. *Int J Nanomedicine* 2023;18:7021–46. https://doi.org/10.2147/IJN.S438307.
56. Xiong D, Gao F, Shao J, Pan Y, Wang S, Wei D, *et al.* Arctiin-encapsulated DSPE-PEG bubble-like nanoparticles inhibit alveolar epithelial type 2 cell senescence to alleviate pulmonary fibrosis via the p38/p53/p21 pathway. *Front Pharmacol* 2023;14:1141800. https://doi.org/10.3389/fphar.2023.1141800.
57. Liu C, Zhao W, Zhang L, Sun H, Chen X, Deng N. Preparation of DSPE-PEG-cRGD modified cationic liposomes for delivery of OC-2 shRNA and the antitumor effects on breast cancer. *Pharmaceutics* 2022;14:2157. https://doi.org/10.3390/pharmaceutics14102157.
58. Yao M, Li M, Peng D, Wang Y, Li S, Zhang D, *et al.* Unraveling macrophage polarization: functions, mechanisms, and "double-edged sword" roles in host antiviral immune responses. *Int J Mol Sci* 2024;25:12078.
59. Dousdampanis P, Aggeletopoulou I, Mouzaki A. The role of M1/M2 macrophage polarization in the pathogenesis of obesity-related kidney disease and related pathologies. *Front Immunol* 2025;15:1534823. https://doi.org/10.3389/fimmu.2024.1534823.
60. Deng A, Fan R, Hai Y, Zhuang J, Zhang B, Lu X, *et al.* A STING agonist prodrug reprograms tumor-associated macrophage to boost colorectal cancer immunotherapy. *Theranostics* 2025;15:277–99. https://doi.org/10.7150/thno.101001.

Downloaded from academic.oup.com/burnstrauma/article/doi/10.1093/burnst/tkag013/8471195 by guest on 12 October 2026

61. Zhao E, Tang X, Li X, Zhao J, Wang S, Wei G, *et al.* Bioactive multifunctional hydrogels accelerate burn wound healing via M2 macrophage-polarization, antioxidant and anti-inflammatory. *Mater Today Bio* 2025;32:101686.
62. Paskeh MDA, Entezari M, Mirzaei S, Zabolian A, Saleki H, Naghdi MJ, *et al.* Emerging role of exosomes in cancer progression and tumor microenvironment remodeling. *J Hematol Oncol* 2022;15:83. https://doi.org/10.1186/s13045-022-01305-4.
63. Xu M, Yang Q, Sun X, Wang Y. Recent advancements in the loading and modification of therapeutic exosomes. *Front Bioeng Biotechnol* 2020;8:586130. https://doi.org/10.3389/fbioe.2020.586130.
64. Zou J, Yang W, Cui W, Li C, Ma C, Ji X, *et al.* Therapeutic potential and mechanisms of mesenchymal stem cell-derived exosomes as bioactive materials in tendon–bone healing. *J Nanobiotechnology* 2023;21:14. https://doi.org/10.1186/s12951-023-01778-6.
65. Li Y, Zhu Z, Li S, Xie X, Qin L, Zhang Q, *et al.* Exosomes: compositions, biogenesis, and mechanisms in diabetic wound healing. *J Nanobiotechnology* 2024;22.
66. Tian H-Y, Liang Q, Shi Z, Zhao H, Altieri F. Exosomal CXCL14 contributes to M2 macrophage polarization through NF-κB signaling in prostate cancer. *Oxidative Med Cell Longev* 2022;2022:1–12.
67. Huang C, Li L, Huang Y, Pang J, Chen G. Advances in targeted modification of extracellular vesicles. *Chin Sci Bull* 2023;68:4532–43. https://doi.org/10.1360/TB-2023-0498.
68. Zou Z, Li H, Xu G, Hu Y, Zhang W, Tian K. Current knowledge and future perspectives of exosomes as nanocarriers in diagnosis and treatment of diseases. *Int J Nanomedicine* 2023;18:4751–78. https://doi.org/10.2147/IJN.S417422.
69. Zhao X, Fu L, Zou H, He Y, Pan Y, Ye L, *et al.* Optogenetic engineered umbilical cord MSC-derived exosomes for remodeling of the immune microenvironment in diabetic wounds and the promotion of tissue repair. *J Nanobiotechnology* 2023;21:176. https://doi.org/10.1186/s12951-023-01886-3.
70. Wu S, Zhang Y, Hou Y, Zhu J, Yang H, Cui Y. Research on the role of exosomes secreted by immortalized adipose-derived mesenchymal stem cells differentiated into pericytes in the repair of high glucose-induced retinal vascular endothelial cell damage. *Exp Eye Res* 2024;247:110046.
71. He G-H, Dong M, Chen S, Wang Y-C, Gao X, Wu B, *et al.* Mesenchymal stem cell-derived exosomes inhibit the VEGF-A expression in human retinal vascular endothelial cells induced by high glucose. *Int J Ophthalmol* 2021;14:1820–7. https://doi.org/10.18240/ijo.2021.12.03.
72. Xia T, Yu J, Du M, Chen X, Wang C, Li R. Vascular endothelial cell injury: causes, molecular mechanisms, and treatments. *MedComm* 2025;6.
73. Hwang HJ, Kim N, Herman AB, Gorospe M, Lee J-S. Factors and pathways modulating endothelial cell senescence in vascular aging. *Int J Mol Sci* 2022;23:10135. https://doi.org/10.3390/ijms231710135.
74. Halurkar MS, Wang J, Chen S, Bihl JC. EPC-EXs improve astrocyte survival and oxidative stress through different uptaking pathways in diabetic hypoxia condition. *Stem Cell Res Ther* 2022;13:91. https://doi.org/10.1186/s13287-022-02766-7.
75. Vorotnikov AV, Khapchaev AY, Nickashin AV, Shirinsky VP. *In vitro* modeling of diabetes impact on vascular endothelium: are essentials engaged to tune metabolism? *Biomedicines* 2022;10:3181.
76. Guo X, Wang J, Su R, Luo D, Zhao K, Li Y. Repair effect analysis of mesenchymal stem cell conditioned media from multiple sources on HUVECs damaged by high glucose. *Clin Proteomics* 2024;21:69. https://doi.org/10.1186/s12014-024-09521-5.
77. Yang B, Dong Y, Shen Y, Hou A, Quan G, Pan X, *et al.* Bilayer dissolving microneedle array containing 5-fluorouracil and triamcinolone with biphasic release profile for hypertrophic scar therapy. *Bioact Mater* 2021;6:2400–11. https://doi.org/10.1016/j.bioactmat.2021.01.014.
78. Bravo B, Correia P, Gonçalves Junior JE, Sant'Anna B, Kerob D. Benefits of topical hyaluronic acid for skin quality and signs of skin aging: from literature review to clinical evidence. *Dermatol Ther* 2022;35:e15903. https://doi.org/10.1111/dth.15903.
79. Abatangelo G, Vindigni V, Avruscio G, Pandis L, Brun P. Hyaluronic acid: redefining its role. *Cells* 2020;9:1743.
80. Roehrs H, Stocco JGD, Pott F, Blanc G, Meier MJ, Dias FAL. Dressings and topical agents containing hyaluronic acid for chronic wound healing. *Cochrane Database Syst Rev* 2023;7:CD012215. https://doi.org/10.1002/14651858.CD012215.pub2.
81. Silvestro I, Lopreiato M, Scotto, d'Abusco A, Di Lisio V, Martinelli A, Piozzi A, *et al.* Hyaluronic acid reduces bacterial fouling and promotes fibroblasts' adhesion onto chitosan 2D-wound dressings. *Int J Mol Sci* 2020;21:2070. https://doi.org/10.3390/ijms21062070.
82. Cho JR, Lee M-H, Oh H-K, Kim H, Kweon D-K, Kang SM, *et al.* Efficacy of hyaluronic acid film on perianal wound healing in a rat model. *Ann Surg Treat Res* 2021;101:206–13. https://doi.org/10.4174/astr.2021.101.4.206.
83. Zhang L, D'Amora U, Ronca A, Li Y, Mo X, Zhou F, *et al. In vitro* and *in vivo* biocompatibility and inflammation response of methacrylated and maleated hyaluronic acid for wound healing. *RSC Adv* 2020;10:32183–92. https://doi.org/10.1039/d0ra06025a.
84. Jin W, Li Y, Yu M, Ren D, Han C, Guo S. Advances of exosomes in diabetic wound healing. *Burns Trauma* 2025;13:tkae078. https://doi.org/10.1093/burnst/tkae078.
85. Huang K, Mi B, Xiong Y, Fu Z, Zhou W, Liu W, *et al.* Angiogenesis during diabetic wound repair: from mechanism to therapy opportunity. *Burns Trauma* 2025;13:tkae052. https://doi.org/10.1093/burnst/tkae052.
86. Yang P, Lu Y, Gou W, Qin Y, Zhang X, Li J, *et al.* Andrias davidianus derived glycosaminoglycans direct diabetic wound repair by reprogramming reparative macrophage glucolipid metabolism. *Adv Mater* 2025;37:e2417801. https://doi.org/10.1002/adma.202417801.
87. Huang Z, An H, Guo H, Ji S, Gu Q, Gu Z, *et al.* An asymmetric natural nanofiber with rapid temperature responsive detachability inspired by Andrias davidianus for full-thickness skin wound healing. *Adv Fiber Mater* 2024;6:473–88. https://doi.org/10.1007/s42765-023-00364-7.

Downloaded from academic.oup.com/burnstrauma/article/doi/10.1093/burnst/tkag013/8471195 by guest on 12 October 2026

© The Author(s) 2026. Published by Oxford University Press. This is an Open Access article distributed under the terms of the Creative Commons Attribution-NonCommercial License (https://creativecommons.org/licenses/by-nc/4.0/), which permits non-commercial re-use, distribution, and reproduction in any medium, provided the original work is properly cited. For commercial re-use, please contact reprints@oup.com for reprints and translation rights for reprints. All other permissions can be obtained through our RightsLink service via the Permissions link on the article page on our site—for further information please contact journals.permissions@oup.com.
Burns & Trauma, 2026, 14, tkag013
https://doi.org/10.1093/burnst/tkag013
Research Article